1 **Title:** Perceptual processing of tastes is performed by the amygdala-cortical loop

2 **Abbreviated title:** The amygdala-cortical loop processes taste

3 **Authors:** Mahmood, A.[1,2], Steindler, J.R.[3], Katz, D.B.[1,2]

4 Department of Psychology[1], Volen Center for Complex Systems[2], Brandeis University, Waltham, MA

5 Lewis Katz School of Medicine[3], Temple University, Philadelphia, PA

6 **Corresponding Author:** Donald B. Katz, dbkatz@brandeis.edu

7 **Conflicts of Interest:** None declared

Contents

Abstract 3
Significance Statement 4
Introduction 5
Results 8
Overview 8
During taste processing, BLA and GC population firing rate transitions happen with zero lag 10
BLA-GC interaction dynamics are asymmetric but time-locked 13
Poisson Generalized Linear Model reveals overlapping groups of GC neurons influencing and influenced by BLA neuron activity 20
Taste processing in GC is a function of embeddedness in the amygdala-cortical loop 27
Discussion 30
Amygdala-cortical taste activity evolves as a joint attractor network 31
Results from research on other sensory systems are consistent with these conclusions 32
The function(s) of BLA-GC directional influences 33
The role of projection neurons in sensory processing 34
Conclusion 36
Methods 38
Experimental Design and Statistical Analyses 38
Subjects 38
Electrode and intra-oral cannula construction 38
Surgery 39
Acquisition of electrophysiological data 39
Habituation and passive taste administration 39
Histology 40
Data and statistical analyses 41
Local Field Potential processing and analysis 41
Analysis of Spiking Activity 44
Changepoint Modeling of Population Activity 46
Generalized Linear Modelling 47
Data Availability 49
References 50

Abstract

Reciprocal connectivity, which generates nonlinear dynamics within a system, should do the same in the taste circuit, which is rife with between-region feedback. Much evidence supports the existence of specific, characterizable within-region dynamics in taste processing, but scant attention has been paid to dynamic inter-region interactions in taste processing. To fill this gap, we apply investigate simultaneous recordings from rodent Gustatory Cortex (GC) and Basolateral Amygdala (BLA), testing specific hypotheses about reciprocal amygdala-cortical interactions. We find that initially GC and BLA responses are independent, but evolve into synchronous, zero-lag ensemble transitions (surprising given the long axons connecting the two regions) within a few hundred milliseconds of taste delivery. Spectral Granger Causality (which infers directional influences) revealed that this tight synchrony also characterizes the system's asymmetric inter-region influences wherein the BLA→GC influence is dominant prior to the generation of the behavioral response and the GC→BLA influence becomes strong at the time that GC has been shown to release a behavior-relevant signal. To better understand the function of single neurons in this process, we then used Poisson Generalized Linear Modeling to categorize GC neurons in terms of their inferred connectivity. This analysis revealed that GC neurons that both influence and receive influence from BLA—the neurons most deeply embedded in the reciprocal circuit—are the ones most strongly involved in taste processing (quantified as taste-specificity and palatability-relatedness). These results, which are consistent with findings in multiple systems and species, support the notion that taste processing is a function of the amygdala-cortical loop.

Significance Statement

Consensus is growing that taste (and other sensory) circuitry should be considered as dynamical systems; this theoretical stance requires studying reciprocal interactions. Building on previous work on dynamic cortico-amygdalar interactions, here we show that in response to taste stimuluation, BLA and GC (following an initial transient) coalesce into a single processing network with zero-lag population state transitions; within this unified structure, GC and BLA “take turns” influencing one another. We go on to show, in single-neuron analyses, that taste processing is a function of the amygdala-cortical loop—neurons that are most deeply embedded in that loop are those that code taste most strongly. In sum, this research suggests a unified framework for conceptualizing the evolution of sensorimotor transformation in general.

Introduction

The taste circuit, like those supporting the other senses, is not a feedforward processing stream; rather, most pairs of regions involved in taste processing are reciprocally connected (1–3). Thus, each region receives feedback from its targets at the same time that it influences those targets, a fact that should cause the system to express nonlinear dynamics when activated (4–6). Specifically, several specific, novel predictions can be made about taste processing within pairs of reciprocally-connected regions: 1) that each region should "code" tastes dynamically; 2) that these regions should become "coupled" into single processing units when activated by tastes; 3) that taste processing should involve highly dynamic "conversations" between coupled pairs of brain regions; and 4) that single neurons' involvement in taste processing should depend upon being a part of that conversation—i.e., being embedded within the task-relevant reciprocal circuit.

While the roles/functions of individual brain regions in taste processing have been extensively investigated—investigation which has produced ample evidence for hypothesis 1 above (see below)—the impact of reciprocal circuitry on interactive processing among these regions (hypotheses 2-4) have received far less study. Only a small set of experiments has investigated the impact that perturbations of neural activity in one region have on firing in another (7–12), and a smaller number have analyzed simultaneous electrophysiological recordings from multiple regions (13–16). In general, these studies support the hypothesis that between-region interactions have a role to play in taste and taste learning (as also appears to be the case in other systems). Because they have without exception used simple, non-directional correlation measures, however, these studies were unable to investigate hypotheses related to the "ebb-and-flow" of directed inter-regional influences. Asymmetries (17–21) and dynamics of interaction (4,22,23) have been profitably studied in other sensory and decision-making systems, but the kinds of techniques used in these

studies have not yet been applied to taste processing. In sum, previous work on inter-region interactions in taste processing has left largely unaddressed questions regarding which regions and neuronal populations exert specific influence on other regions, when in real time they do so, and what the implications of these interactions might be for our understanding of taste processing.

We have recently begun an investigation into such real-time interactions, focusing on the two most prominently discussed nodes of the forebrain taste circuit—basolateral amygdala (BLA) and gustatory cortex (GC, 16). During tasting, neural responses in both structures show evidence of nonlinear dynamics, in that they progress through a sequence of distinct processing states (24,25) separated by sudden, coherent ensemble transitions (16,26; see Fig. 1A); furthermore, activity in the two regions becomes correlated (at the level of single-neuron pairs and population activity) during production of these sequences (16), a result suggesting that BLA and GC may form part of an attractor network (5,27,28). Thus, these responses likely reflect reciprocal BLA-GC interactions (*via* BLA→GC and GC→BLA axonal projections; 29–32) involved in processing tastes.

Here we leverage this current understanding of taste response dynamics to generate novel insights into the systemic nature of taste processing. We first demonstrate that BLA and GC are operating on a single "processing clock"—despite relatively lengthy axons separating the structures, ensemble firing rate transitions occur with zero between-region lag. Spectral Granger Causality brought to bear on simultaneously-recorded local field potentials (LFP) provides converging evidence of this time-locking of inter-regional dynamics, but also shows that the influence that BLA exerts on GC during particular epochs of the response differs from the "feedback" influence: in the μ/α frequency band (2-12 Hz), processing across the period of taste processing is dynamic, with BLA influencing GC during the 300-1000ms post-stimulus delivery period—the state during which BLA responses are palatability-related (13,16,25), and just before GC responses become so (26,33); GC influence on BLA in this frequency band, meanwhile, peaks only briefly at the end of this period (approx. 1000ms

118 following stimulus delivery), around the time of the transition into the state in which GC emits
119 behavior-related signals (34).

120 Finally, we connected these results back to spiking in single neurons using Poisson Generalized
121 Linear Modeling (pGLM), which allows us to divide our GC sample into distinct neural subpopulations
122 based on whether they influence BLA, are influenced by BLA, or both. Analysis of this functional cell-
123 type division revealed that GC neurons with taste responses that are influenced by BLA activity show
124 significantly more taste-specific and palatability-related firing than neurons that do not, and that
125 neurons that both influence and receive influence from BLA exhibit the strongest taste specificity and
126 palatability-relatedness. That is, our results demonstrate that the degree to which a GC neuron is
127 embedded in the reciprocal circuit largely determines its involvement in taste processing.

Results

Overview

Our analysis of amygdala-cortical taste responses has 3 parts, beginning with an evaluation of between-region lags in the times of the 3 sudden ensemble firing-rate transitions that characterize the evoked taste-response, and the finding that all but the 1st transition are essentially simultaneous in BLA and GC. The simultaneity of these later transitions shows that BLA and GC become coupled while processing tastes, such that by the onset of palatability-related firing in GC (at the latest), they are essentially showing no sign of the reliable delays that would be expected if these sudden firing rate changes were being "transmitted" from one region to the other *via* between-region axons.

This finding does not, however, imply that BLA and GC necessarily play identical roles in taste processing, any more than the fact that two individuals engaged in a single real-time conversation are necessarily saying the same thing. We therefore go on to use Spectral Granger Causality—a tool that essentially breaks down the degree and timing of each region's influence on activity in the other (in each frequency band)—to test for "asymmetries" in BLA-GC communication, by which we mean differences between BLA's influence on GC and GC's influence on BLA (note that we use the term "influence" to reflect in general terms the fact that one region's activity influences the other, without claiming additional mechanistic insight such as a distinction between direct and indirect projections or excitatory and inhibitory connections). This analysis revealed that the strength of the GC→BLA influence is continuously high in frequency bands above 20 Hz; the oft-described taste processing dynamics, meanwhile, "live" exclusively in asymmetries of influence observed in the μ/α band (i.e., below 12 Hz; (15,35–37), where BLA influences GC during the 300-1000ms post-stimulus delivery—the "middle epoch," during which BLA firing is palatability-related and GC's is not (**Fig. 1A**, and see

11,15,16,24,34,38)—and GC briefly influences BLA just afterward, at the moment that the GC response becomes palatability-related in a transition of firing that has been shown to influence behavior (34). These direction-specific influences, however distinct, change in near-perfect lock-step, providing converging evidence that the two regions are behaving as a single processing unit.

To better assess the functional implications of these results, we then use Poisson Generalized Linear Modeling to conservatively identify single neurons with inter-regional influence—GC neurons that influence activity in BLA, GC neurons that are influenced by activity in BLA, and neurons that do both. We then evaluated the taste responses of the functionally defined neuron groups; these analyses reveal that involvement in taste processing is determined by the degree to which a neuron is embedded in the reciprocal interaction between the two structures, with GC neurons that both influence and receive influence from BLA showing the largest magnitudes of both taste-specific and palatability-related taste responses.

During taste processing, BLA and GC population firing rate transitions happen with zero lag

Our overarching hypothesis is that BLA and GC, both of which undergo multiple ensemble firing-rate transitions during taste responses (16), can be reasonably described as functioning as a single, distributed network (5,27,28,39–41). Such a hypothesis generates the specific prediction that these firing-rate transitions should be simultaneous in the two regions (i.e., there should be zero between-region lag), because the transitions in an attractor network are generated by coordinated activity of the regions with no specific "sources" or "epicenters" of the transitions. If BLA and GC cohere into a single network, the oft-described transitions in ensemble firing rates that make up taste responses in both regions (16,34,38,42) aren't expected to originate in either one, but rather to emerge within the network as a whole (28,40). If, on the other hand, transitions either spread from one region to the other or are generated in a source common to the two, one would likely observe a consistent non-zero lag structure (see Discussion). Having shown (16) that transition latencies in GC and BLA are correlated, here we begin by testing the prediction that these transitions are zero-lag.

To test this prediction, we apply a model that infers states and state-transitions in stimulus-driven activity to each region independently (16,26,38,42). This analysis shows that such transitions occur in the expected time ranges: in each region and trial, a first transition appears at 300±250ms following taste delivery (but see below), a second at 850±300ms following taste delivery, and a third at 1450±325ms following taste delivery (mean±std, rounded to the closest 25ms for clarity). As shown previously, the precise timing of these transitions varies widely from trial to trial.

Fig. 1A, which summarizes the basic taste-processing dynamics that have been identified in GC and BLA (16,25), identifies the transitions as they are used throughout these figures. **Fig. 1B** is a

186 schematic of the analysis comparing the timing of these lags, and **Fig. 1C** shows the distributions of
187 calculated GC-BLA lags for each transition. Examination of **Fig 1Ci**, which presents the distributions
188 for each individual session as a heat map, suggests that the between-region lags tend to be highly
189 reliable across the 18 sessions (from 6 rats), appearances that are confirmed by the tightness of the
190 distributions of mean between-region lags for each session and transition (**Fig 1Cii**). Analysis of these
191 latter distributions reveals that, for the earliest transition, sudden changes in BLA ensemble firing
192 rates tend to lead those in GC by ~100ms (permutation test, 95%CI=[57, 183], $p<0.001$); we were
193 unable, however, to identify significant between-region lags for the following two transitions
194 (permutation test, Transition 2: 95%CI=[-74.5, 51.5], $p=0.78$; Transition 3: 95%CI=[-86, 39.5],
195 $p=0.43$). When we, as a further test, compared the distribution of average lags across transitions,
196 transitions 2 and 3 both proved to be significantly different from transition 1 (1 vs. 2: $p=0.001$, 1 vs. 3:
197 Wilcoxon signed-rank test, $p=0.015$), the average lags for transitions 2 and 3, meanwhile, were not
198 significantly different from each other (Wilcoxon signed-rank test, $p=0.747$). These data therefore
199 suggest that, after beginning their taste responses at different times, BLA and GC become not only
200 coupled but synchronized, undergoing essentially simultaneous transitions into (and out of) the GC
201 palatability-related state (**Fig. 1A**; see below for convergent evidence).

202 This pattern of results supports the hypothesis that BLA and GC, rather than being a joint processing
203 network "at rest," coalesce into a dyad only after producing uncoordinated initial transients in their
204 taste responses. The lag present in the first transition suggests that BLA and GC taste responses are
205 initially driven independently, although there are other possible explanations; regardless, this initially
206 uncoupled activation gives way to the two regions cycling through the later transitions of their taste
207 responses as a single processing unit, such that the relatively long axons connecting the two regions
208 fail to induce delays in the firing-rate transitions that characterize taste processing (see Discussion).

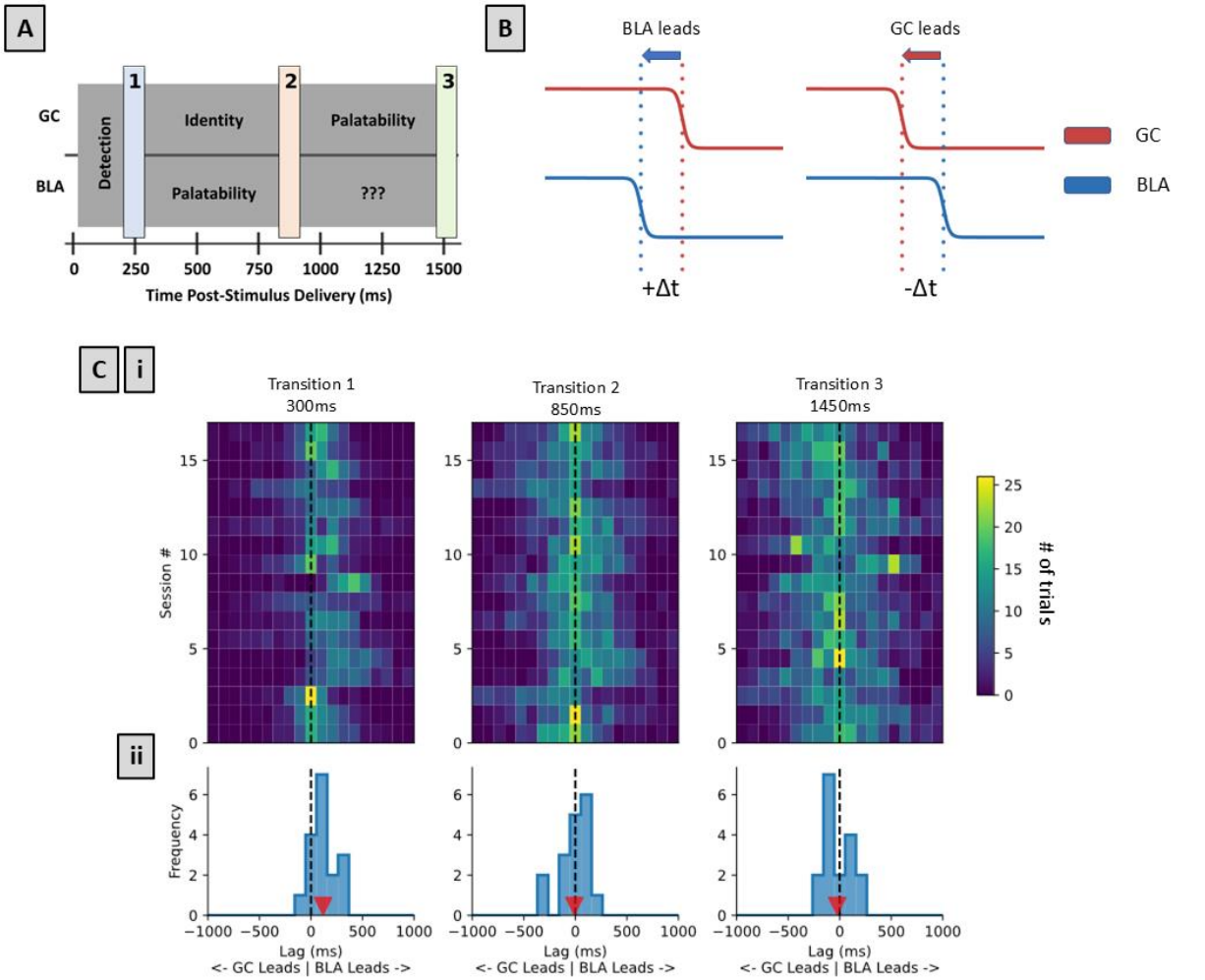

Fig 1. BLA initially leads GC in state transition but both regions subsequently show zero-lag coordination. A) Summary schematic of the timing and "coding content" previously demonstrated to characterize state sequences in GC and BLA ensemble spiking activity. Overlain are the numbers used in this study to label these transitions. **B)** A schematic illustrating how transition lags between GC and BLA were calculated and how we define the sign of the lags. **Ci)** Distributions of transition lags, presented as heat maps (legend at right shows the # of trials with a specific transition lag) for 18 sessions (y-axis) across 6 animals for each of the 3 transitions. **Cii)** Summary distributions of lags for each transition, with red arrows indicating the grand-average lag. The significance of the

difference between that grand-average lag and 0 was evaluated using bootstrapped 95% confidence intervals of the distribution mean (see text).

BLA-GC interaction dynamics are asymmetric but time-locked

Even seamless zero-lag coupling of firing-rate transitions in BLA and GC does not necessarily imply that each has identical influence on the other, any more than a deduced general function of a single brain region negates the possibility of differences between the action of distinct subpopulations of neurons. Rather, it implies only that the degree to which one region influences the other should be dynamic, and that any such dynamics of this influence should occur in concert with dynamics in the feedback influence (see Discussion for consideration of other coupled systems in which asymmetric patterns of influence nonetheless evolve in concert). With that in mind, any complete understanding of the function of this amygdala-cortical dyad will necessarily involve an examination of the dynamics of directional influence—of the moment-to-moment degree to which activity in each area impacts activity in the other.

We performed this examination by applying Spectral Granger Causality (GrCa) to LFPs recorded from BLA and GC. Rather than simply assessing similarity between timeseries as a measure of coordination (as done in a cross-coherence or correlational analysis), GrCa allows us to disentangle directional dependencies by making use of time-lagged regressions: in essence, GrCa assumes that if the future of timeseries A is better predicted using both the histories of timeseries A and B (compared to just using the history of timeseries A), then B can be thought to “causally” influence the future of A (43,44) broken down by frequency (45–47). Use of GrCa allows us to obtain a time-resolved view (a “big-picture” view, owing to the use of LFPs as a signal) of the dynamics of interaction between BLA and GC. Significance of influence in GrCa can then be assessed for each time and frequency bin.

241 **Fig. 2** shows the output of this analysis brought to bear on simultaneously recorded GC and BLA local
242 field potentials. Collapsed across time, the influences of the regions on one another are almost
243 entirely contained within the 1-60Hz range (**Fig. 2A**; note that the low-pass filter used when collecting
244 the LFPs allows for the detection of influence well above 60Hz, see Methods), and quite distinct from
245 one another within that range (**Fig. 2B**): GC→BLA influence, while above zero across this entire range
246 of frequencies, is highest (and dominant) from 20 to 60Hz (the β and γ frequency ranges; see Buzsáki
247 and Draguhn, 2004); BLA→GC influence, meanwhile, which is essentially non-existent (and non-
248 significant) across most of the β/γ range, is dominant in frequencies (2-12Hz, the θ and μ range, the
249 latter of which is sometimes referred to as α) which are known to be both particularly prominent in
250 GC evoked activity and modulated in a manner related to the dynamics of GC taste responses (35–
251 37).

252 We note that it is unlikely that this relatively clean separation in directional frequencies is an artifact
253 of the methodology, as GrCa can appropriately recognize influences in identical or overlapping
254 frequency bands (18,19,43,49). Furthermore, the distinctness between the frequency bands of the
255 BLA→GC and GC→BLA influences aligns with previous work showing that pharmacological
256 inhibition of taste thalamus reduces GC LFP power in the 20-60Hz band, but increases it in the 2-
257 12Hz band (15)—a finding that suggests that the 2-12Hz band may be the "channel" for amygalo-
258 cortical interaction, whereas the 20-60Hz band may be the "channel" for the thalamo-cortical
259 interaction (19,20, see Discussion).

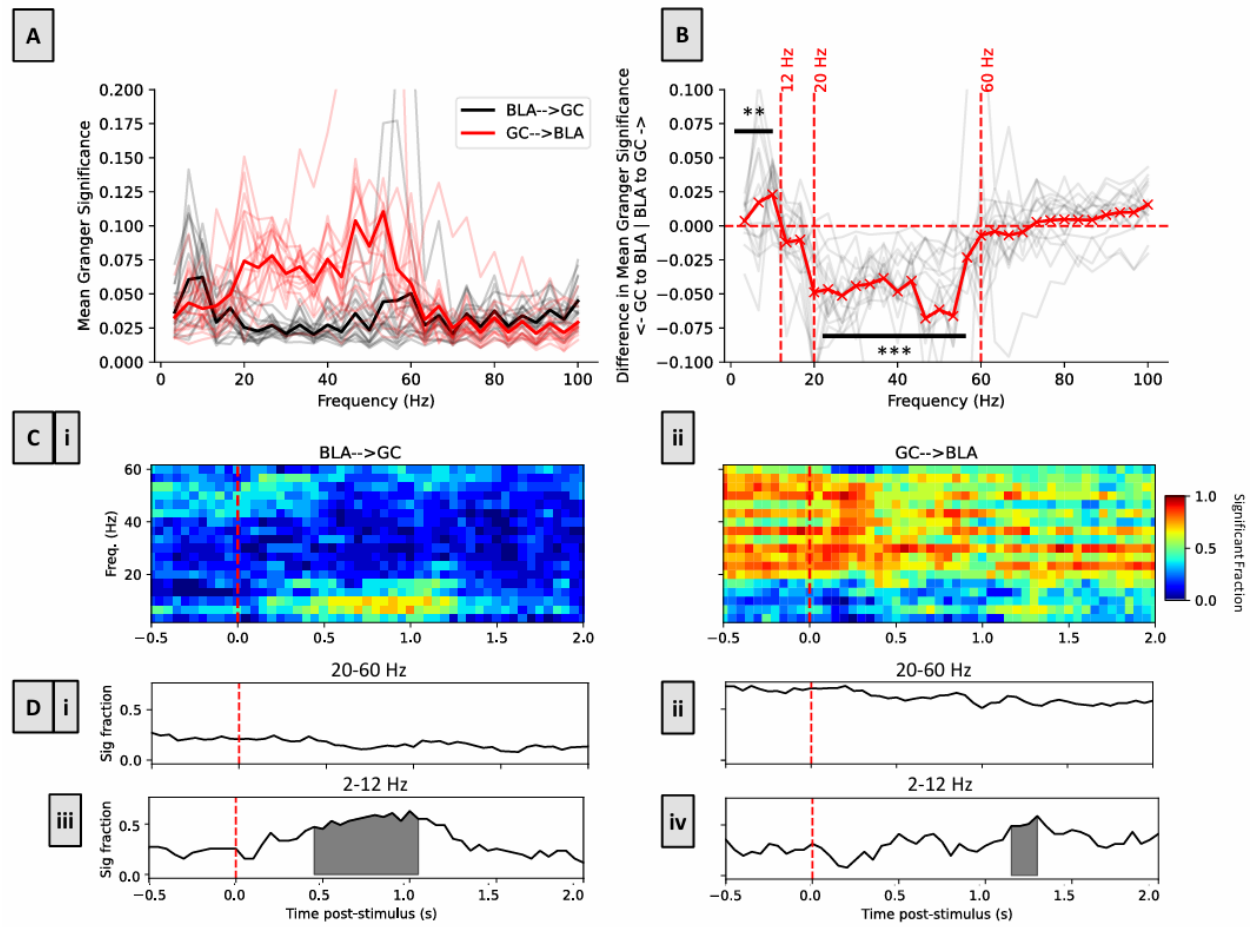

Fig. 2) GC-BLA interaction shows processing-related asymmetries and dynamics. A) Mean (bold lines) and individual sessions' (thin lines) significance of Spectral Granger Causality for 0-2000ms post-stimulus activity across datasets for BLA→GC (black) and GC→BLA (red) influences. **B)** Directional differences in mean (bold red line) and individual subjects' (thin black lines) influence across frequency bands for data shown in A). Above-zero differences mean stronger BLA→GC influence, and below-zero differences mean stronger GC→BLA influence. BLA→GC is stronger below 12Hz, and GC→BLA dominates between 20 and 60Hz; ** = $p<0.05$, *** = $p<0.005$ **C)** The data from Fig. 2A unpacked into significant time-frequency bins for **i**) BLA→GC and **ii**) GC→BLA influence. Brighter color indicates that a larger fraction of the recording sessions displayed significant Granger Causality at that time-frequency bin (heatmap legend to right). In both panels the difference between

higher and lower frequency bands can be seen, and across panels the asymmetry in influence can be seen; furthermore, dynamics of influence are apparent in the lower frequency band. **D)** The data shown in C collapsed across frequencies within each identified bandwidth (frequency band limits are given above each panel). Dynamics of influence are restricted to the <12Hz bandwidth; shaded regions indicate periods of strongest significance determined using cluster-permutation testing. See text and Methods for more details.

277 This difference between low and high frequencies is easily seen in plots of the significance of
278 direction-specific influence through time (**Fig. 2C**; compare the upper two thirds to the lower third in
279 each panel), as is the difference between GC→BLA and BLA→GC influence (compare the left and
280 right panels). This presentation further suggests that, in general, β/γ influence may be slightly higher
281 spontaneously than during taste processing, and that the differences between BLA→GC (**Fig. 2Ci**)
282 and GC→BLA (**Fig. 2Cii**) influence in θ/μ frequencies change repeatedly across taste processing
283 time—that they reflect the oft-described GC dynamics.

284 To rigorously assess these seeming phenomena, we plotted the average proportion of sessions in
285 which power in each frequency-time bin is significantly above zero (the "significant fraction") in each
286 direction of influence, collapsed across the frequencies within the two dominant bands. This
287 analysis reveals near-tonic influences in the higher frequency band (**Fig. 2Di** and **ii**; the average
288 GC→BLA magnitude of influence is of course higher than that of BLA→GC influence), although there
289 is a slight trend toward a reduction of influence following taste delivery. The μ/α band results,
290 meanwhile, accord well with our understanding of the known GC taste-response dynamics (**Fig. 2Diii**
291 and **iv**). In each panel, the shaded regions represent the result of cluster-based permutation testing,
292 identifying the longest continuous periods in which this result is significantly higher than that of
293 randomized data (there are no such periods in **Fig. 2Di/ii**). With regard to BLA→GC influence in the
294 lower frequency band (**Fig. 2Diii**), this period is a good match to the average GC identity epoch
295 (approx. 300-1000ms post-stimulus, see **Fig. 1A**). Given that BLA responses are palatability-related
296 during this period, and that GC responses become palatability-related only at the end of this period,
297 this result also accords well with classic studies on the role of amygdala in stimulus valuation, which
298 have led both human and rodent researchers to theorize that amygdala "passes" emotional valence
299 to cortical regions (7,11,51,52, see also Discussion). GC→BLA influence in this frequency range,
300 meanwhile (**Fig. 2Div**), peaks only briefly at the end of this BLA→GC push. This finding further

301 corroborates the above interpretation, suggesting that GC, after being influenced by BLA, emits
302 decision-related activity capable of influencing behavior, and as such it is also consistent with work
303 demonstrating that the transition into palatability-related firing in GC (which typically occurs around
304 this time) is causally linked to the driving of behavior (26,34).

305 Again, the fact that this amygdala-cortical interaction dynamic is asymmetric, in that BLA strongly
306 influences GC during a period of post-stimulus time in which GC does not influence BLA (and vice
307 versa), was not unexpected. If the two regions truly form a recurrently connected system, however,
308 one would further expect that even these asymmetries of influence should run on the same "clock"—
309 that is, that changes in influence should occur simultaneously. To test this hypothesis, we performed
310 Principal Component Regression on each time-series shown in **Fig. 2C**. **Fig. 3A** illustrates the
311 trajectories for the data in the two Fig. 2C panels obtained from this regression overlain on one
312 another. The dynamics of the two timeseries, which are visualized as changes in the trajectories'
313 directions through space, are clearly very similar. We quantified this seeming similarity by assessing
314 the mean-squared error (MSE) of linearly predicting one time-series from the other (**Fig. 3B**, red
315 dashed line) compared to that produced by the same linear regression of the two time-series after
316 shuffling them temporally (linear, inter, shuffled), and also by linear and non-linear (i.e., using multi-
317 layered artificial neural network) auto-regression (i.e., predictions of each time series from itself; see
318 Methods) to give us a lower-bound for prediction error. The results of these analyses make it clear
319 that the linear prediction of the BLA→GC time-series from the GC→BLA time-series was almost as
320 accurate as the non-linear auto-regression and better than the linear auto-regression (this was not
321 surprising given the nonlinearities in the BLA-GC interaction dynamics). Simply put, the inter-series
322 prediction nears the limit of prediction accuracy, a fact that serves as converging evidence for our
323 hypothesis that BLA and GC form, upon receiving taste input, a single distributed dyad with time-

locked, coupled dynamics—albeit dynamics within which GC→BLA and BLA→GC influences are asymmetric.

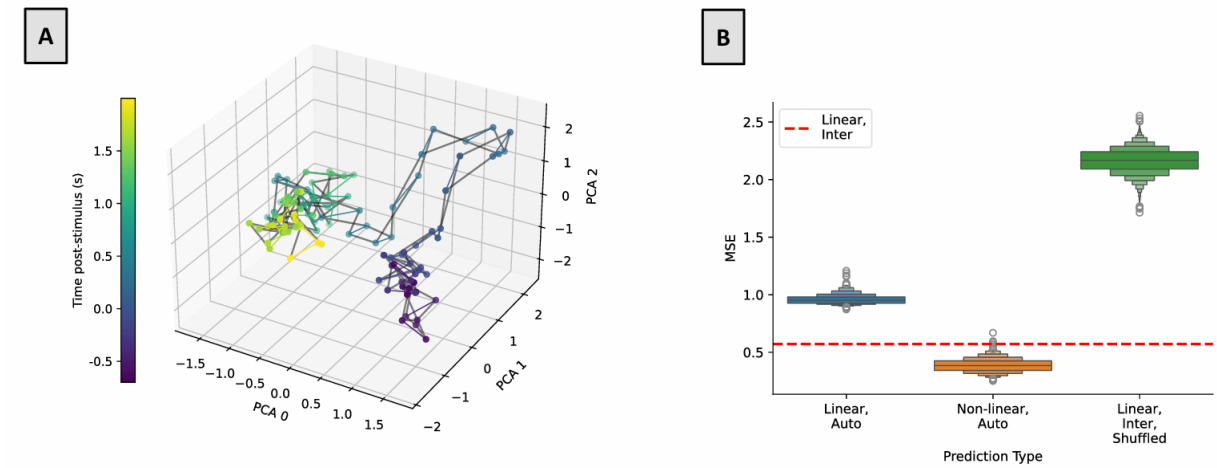

Fig. 3) Dynamics of BLA→GC and GC→BLA influences are time-locked. A) Aligned principal components of spectra shown in **Fig. 2C**, indicating that the dynamics of BLA→GC and GC→BLA influence are strongly coordinated, in that the trajectories change direction together through time. Elapsing post-stimulus time is shown with changing colors (legend to left), and taste delivery time is shown as a red dot. **B)** Quantification of alignment shown in A). Prediction of one time-series (GC→BLA) from the other (BLA→GC) using linear regression (Linear, Inter) is better than both shuffled linear regression (Linear, Inter, Shuffled), and linear autoregression (Linear, Auto) of timeseries, and almost as good as non-linear autoregression (Non-linear, Auto).

Poisson Generalized Linear Model reveals overlapping groups of GC neurons influencing and influenced by BLA neuron activity

As noted above, the finding that different patterns of influence appear to "live" in different frequency bands is not without precedent—bottom-up and top-down influences in visual pathways have also been suggested to segregate into separate frequency bands (18,19,53). Meanwhile, the fact that BLA→GC influence is focused in the 2-12Hz range is intriguing, given previous studies showing that GC taste-processing dynamics are also prominently visible in GC μ activity (15,35–37): these facts add to the evidence that BLA and GC become a single dynamical object while processing tastes, further motivating our hypothesis that the involvement of GC neurons in taste processing (which can be quantified in terms of the magnitude of GC responses' taste-specificity and palatability-relatedness) might be a function of their coupling with BLA.

To test this hypothesis, we trained Poisson Generalized Linear Models (pGLM, see Methods for important differences between pGLM and the more commonly-used General Linear Model) to infer connectivity and influence between individual GC-BLA neuron pairs—an aim that cannot be achieved with GrCa (see Methods), and that allows us to categorize individual GC neurons as putatively "sending" and/or "receiving" inter-regional influence (or both). We fit pGLMs to single neurons in our dataset, using spike trains from all other simultaneously recorded neurons as input (54–56). An advantage of this analytic approach to inferring connectivity is that, while it cannot capture the dynamics of influence, it is inherently more conservative than correlational methods such as spike-train cross-coherence (57). This is because stimulus input and the history of spiking in the current neuron "compete" against one another, and with the recent spiking of other neurons (**Fig. 4A**), for significance during pGLM inference. Evoked activity of a neuron can potentially be explained as a function of any of these variables, and therefore only explanatory value above and beyond what

359 is predicted by all other variables is deemed evidence of a functional inter-regional influence—
360 "influence" that can be attributed to other sources is essentially "partialled out." Standard
361 correlational approaches are significantly more prone to false positives due to the shared latent
362 dynamics across neurons within regions and across regions (55).

363 We fit models to 151 GC and 160 BLA well-isolated single neuron waveforms (mean±SD per session:
364 9.4±4.14, GC; 10.0±4.61, BLA). Before we could test our central hypothesis (that taste processing is
365 a function of embeddedness in the amydala-cortical loop), it was first necessary to test whether the
366 models successfully fit the data. Toward that end, **Fig. 4B** shows 2 representative examples of actual
367 PSTHs (left) and PSTHs predicted by the fit pGLMs (right). The apparent similarity between the two is
368 quantified in **Fig. 4C**, which shows that the model consistently produces significantly better fits to
369 the data than models fit on spike-trains shuffled between trials (Wilcoxon signed-rank test, $p <$
370 0.001), a control that preserves the average statistics of the spike-trains used, eliminating only the
371 within-trial coordination of spiking between neurons. This result highlights the fact that, despite
372 significant trial-to-trial variability in spiking, the pGLM learns relationships that are meaningful within
373 trials.

374 As an additional test of the pGLM fits, we also compared correlations between actual PSTHs and: 1)
375 trial-matched predictions; 2) cross-unit predictions; and 3) predictions on circularly shuffled data
376 (**Fig. 4D**, see Methods for details). We find, as expected, that trial-matched predictions (blue
377 histogram and summary box plot) perform best, followed by unit-shuffled/cross-unit predictions (in
378 orange); we suspect that these control correlations were significantly above zero because many GC
379 neuron pairs tend to exhibit broadly similar neural dynamics. Worst were correlations with circularly
380 shuffled (temporally garbled) data, which were essentially zero (in green). Statistical comparisons
381 confirm that trial-matched predictions are significantly better than either control comparison
382 (Wilcoxon signed-rank test, $p<0.001$ for each comparison). Together, these tests allow us to conclude

that the poisson pGLM generates reasonable models of the mechanics (functional circuitry) underlying the observed activity.

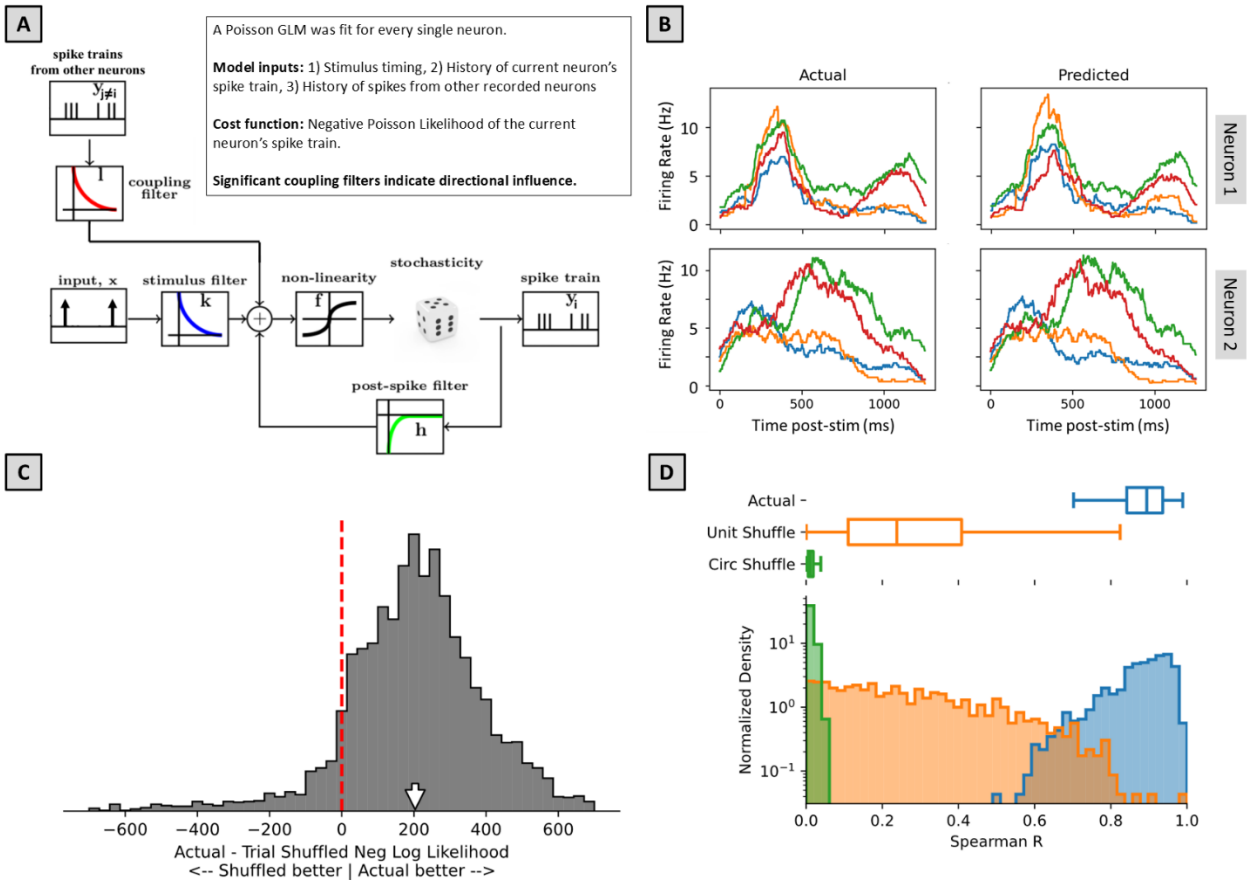

Fig. 4) Generalized Linear Modelling of single-neuron interactions between BLA and GC. A) pGLM structure. Every neuron model depends on: 1) stimulus timing, 2) the neuron's spiking history, and 3) input from (or spiking history of) all other simultaneously recorded neurons. **B)** Actual and Predicted PSTHs of two representative units across 4 delivered tastants (different colors), showing that fitted models (right column) accurately recapitulate single-neuron activity (left column). **C)** The vast majority of models built on real data showed higher cross-validated likelihood than models trained on shuffled data (i.e., the bulk of the distribution is to the right of the vertical red dashed line at equal predictability). This confirms that the models are learning single-trial relevant features. The white arrow indicates the median of the distribution. **D)** The distributions of correlations (Spearman's Rho)

between: 1) actual and predicted PSTHs (blue); 2) unit-shuffled data and prediction (orange); and 3) temporally scrambled data and prediction (Circ shuffle: green).

397 Having established that we can successfully model the amygdala-cortical dataset using pGLM, we
398 moved on to using the model to identify any significant influence of the activity of one simultaneously
399 recorded neuron on that of another (i.e., identifying significant coupling filters). In what follows, we
400 refer to neurons with responses that are concluded to influence activity in the other region as
401 "Output" neurons, and neurons with responses that are concluded to be influenced by activity in the
402 other region as "Input" neurons. **Fig. 5A** shows the distribution of neurons so identified: clearly, our
403 BLA sample contains more Output neurons (40%) than Input neurons (6.3%), with an additional 9.4%
404 categorized as both; the Output and Input populations in GC were more balanced (17.2% and 22.5%,
405 respectively), with an additional 11.9% characterized as doing both. Note that no claim is made
406 about whether these neurons might output to or take input from any structures from which we didn't
407 record, and therefore no further analysis is done on the (probably highly diverse set of) neurons that
408 were categorized as neither Input nor Output.

409 Given the relatively small overlap of Input and Output designations, it was important to ask whether
410 the two groups were structurally distinct—that is, whether a neuron (or neuron type) was specifically
411 likely to be either an Input or Output neuron, but not both. Two separate analyses were performed on
412 this front. First, we performed a direct, Bayesian assessment of the overlap between Output and
413 Input sub-groups in both regions, comparing the data to a null distribution in which labels for
414 connection types were assigned randomly so that we could ask whether, given the likelihood of a
415 neuron being categorized as Input or Output, the conditional probability (i.e., the likelihood of it being
416 categorized as Input given that it was categorized as Output, and vice-versa) was lower or higher than
417 chance. **Fig. 5B** shows that the overlap we observe in the real data falls squarely within the chance
418 probability of overlap for this null-distribution for both regions; we therefore conclude that there is
419 no evidence that Output and Input populations should be thought of as segregated groups.

420 We next assessed the likelihood that the separation of neurons into Output and Input groups aligns
421 with anatomically-defined neuron categories. Specifically, we asked whether putative pyramidal
422 cells, identified on the basis of spike width, were more likely to be Output neurons than Input
423 neurons. **Fig. 5C** demonstrates that our sample of isolated single neurons broke, as expected, neatly
424 into two groups on this basis, with a 0.45ms trough-to-peak time providing a clean cutoff between
425 fast-spiking putative interneurons (Int) and slower-spiking putative pyramidal neurons (Pyr; see
426 (11,58–60). Slightly under 10% of our sample fell into the Int category, a number that is not wildly
427 inconsistent with expectation based on an extensive previous literature using chronic extracellular
428 electrophysiology. Given the small fraction of interneurons, it can be concluded that putative
429 pyramidal neurons are approximately equally likely of being Input and Output neurons. In conclusion,
430 we could find no evidence suggesting that Output and Input neurons are distinct anatomical types
431 (at least at the level of gross subdivision).

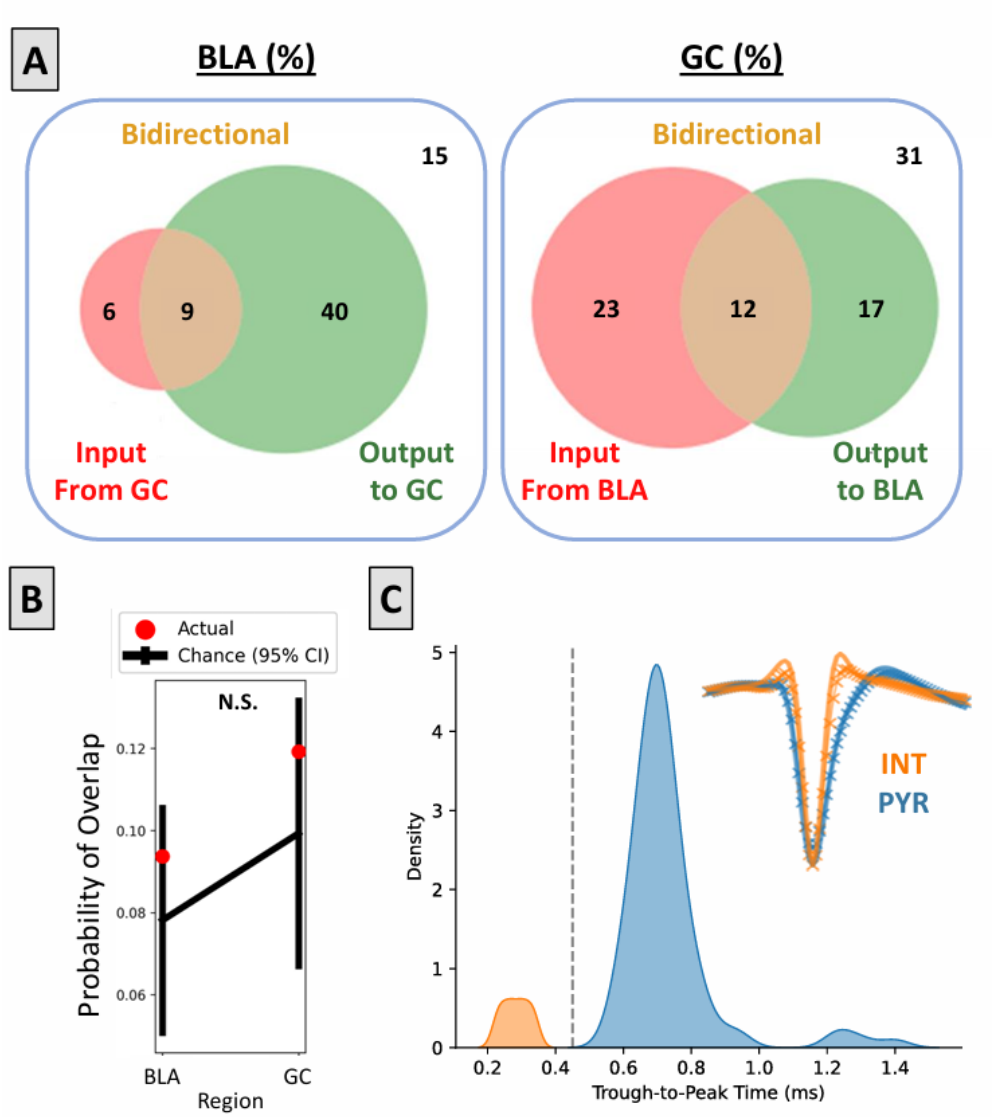

Fig. 5) pGLM brought to bear on amygdala-cortical ensembles identifies functionally (but not structurally) distinct subpopulations of neurons. A) Inference of Input and Output population in the recorded BLA-GC populations (number outside colored circles indicates percentage of neurons with no identified between-region connections). **B)** The amount of overlap between Input and Output populations is not significantly different from that expected by chance in either brain region. **C)** Inferred neuron-types based on trough-to-peak times of waveforms (Inset: solid line = GC, crosses = BLA). Most neurons in the dataset (expectedly) are putative pyramidal neurons, which means that

440 the vast majority (and similar percentage) of each functional neural subtype as shown in panel A is
441 pyramidal.

442 Taste processing in GC is a function of embeddedness in the amygdala-
443 cortical loop

444 While Output and Input neurons do not appear to be separate neuron types, it is nonetheless
445 possible that their positioning within the network causes them to differ with regard to their
446 involvement in taste processing. Next, we tested this possibility; specifically, we tested whether we
447 can discern a relationship between pGLM label and the average magnitude of the neuron's taste-
448 specificity (more distinctive responsiveness to different tastes) and palatability-relatedness
449 (correlation with the hedonic value of the tastants)—the basic variables that describe involvement in
450 taste processing (11,13,16,24–26,33,34,38,61).

451 Initial analyses did in fact reveal significant differences in both taste-coding variables as a function
452 of subpopulation (**Fig. 6A**): GC Input neurons (those shown by pGLM to be influenced by BLA) showed
453 higher magnitudes of both taste specificity and palatability relatedness than did Output neurons.
454 Despite the status of GC as primary gustatory cortex, recipient of ascending taste input from
455 thalamus (2,15,30,62), involvement in taste processing (as measured by taste specificity and
456 palatability relatedness of taste responses) appears to depend on receiving "feedback" input from
457 BLA.

458 As taste discriminability and palatability are (necessarily) semi-redundant and correlated (**Fig. 6B**,
459 Spearman's Rho=0.73, $p<0.001$), it was useful to aggregate and summarize the results shown in **Fig.**
460 **6A** into a single measure. We used for this summary the vector norm (the magnitude of an arrow
461 drawn to a point in 2D-space, see Methods) of normalized discriminability and palatability coding,
462 an aggregate measure of taste-processing involvement that we here refer to as "tastiness." An

463 analysis of neuron tastiness (**Fig. 6C)** confirms the findings of **Fig. 6A**, in that GC Input neurons show
464 significantly higher tastiness than GC Output neurons. Note that these results were not simply an
465 artifact of lower firing rates in the Output neurons, in that we observed no significant link between
466 firing rates and the metrics tested above (Spearman's Rho: Firing Rate vs. Discriminability = 0.1, Firing
467 Rate vs. Palatability = 0.0).

468 The division of responses into Input and Output, which was made without reference to taste coding,
469 effectively reveals the importance of BLA feedback in taste responsiveness. But given that our central
470 hypothesis is that involvement in taste processing depends upon being "embedded" in the
471 amygdala-cortical loop, the most rigorous test involves an analysis of the specific set of neurons that
472 are most deeply so embedded—that is, the GC neurons that are categorized as both influencing and
473 receiving influence from BLA (i.e., "Input/Output" neurons). If our hypothesis is correct, we should
474 expect that these neurons will exhibit the strongest tastiness—even stronger than that of GC Input
475 neurons. Indeed, this proved to be the case: the tastiness of GC Input/Output neurons is significantly
476 higher than that of GC Input neurons (Student's t-test p=0.01), confirming our prediction that the
477 degree of "embedding" in the recursive circuit determines its degree of involvement in taste
478 processing (**Fig. 6C**), a result that is particularly striking given the near total lack of "tastiness" of GC
479 Output neuron responses. The processing of tastes appears to be largely performed by the
480 amygdala-cortical loop as a single dynamical object (see Discussion).

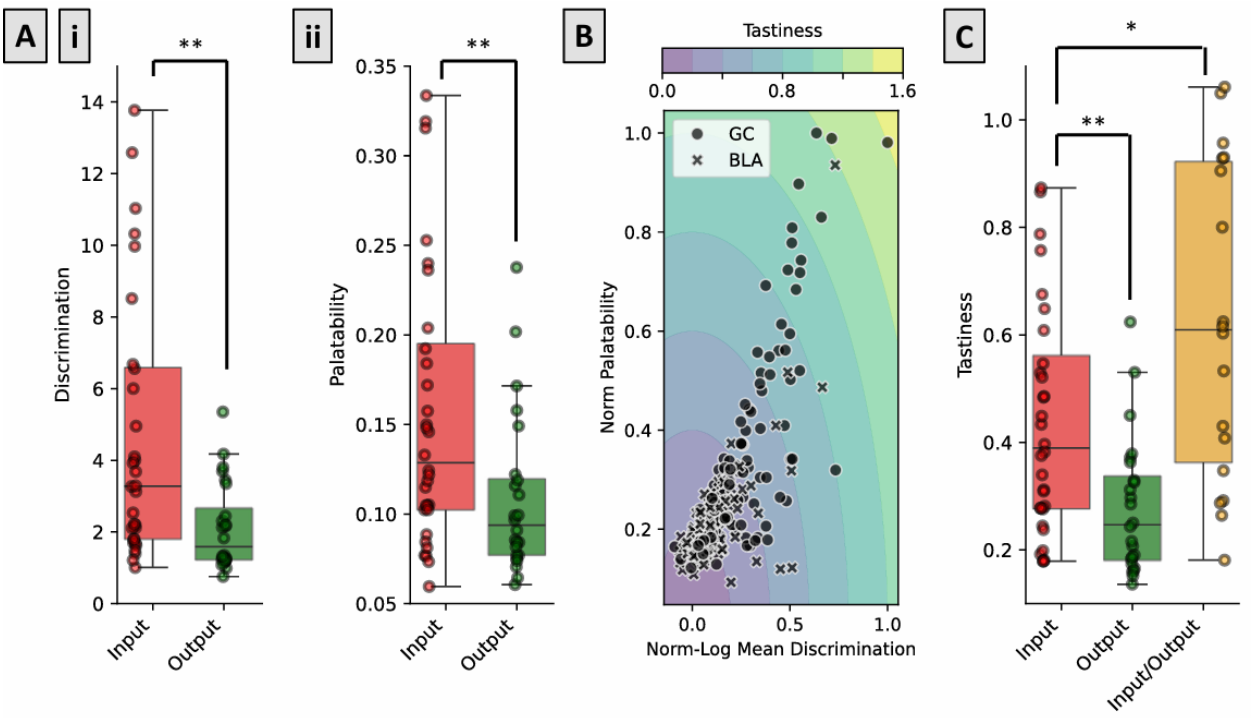

Fig. 6) GC neurons that are embedded in the amygdala-cortical loop are the ones that most strongly process tastes. A) Both taste discriminability **(i)** and palatability-relatedness **(ii)** of GC Input neurons (those influenced by BLA activity), measured in the standard manner (see Methods), are significantly stronger than that in GC Output neurons. ** = p<0.005. **B)** Discriminability and Palatability are significantly correlated for GC neurons (Spearman's Rho=0.73, p<0.001) and hence can be combined into a measure ("Tastiness") that represents a single measure of involvement in taste processing. **C)** Comparison of tastiness among subpopulations confirms the results of A (higher tastiness in Input neurons than Output neurons), but also shows that the small population of GC Input/Output neurons produces responses with significantly higher tastiness than even the Input population (2-sample Student's T-test, ** = p<0.005, * = p<0.05)

Discussion

This study reveals taste processing to centrally involve dynamical activity of the amygdala-cortical loop. Following an initial transient in which they fire independently of one another, BLA and GC respond to taste input with zero-lag coupling of ensemble transitions; within this tight coupling, the flow of influence between the two structures is asymmetric (as assessed using spectral granger causality), even as those differences in influence change synchronously. Put simply, BLA and GC become a single dynamical system, such that any individual GC neuron's involvement in taste processing—measured in terms of the taste-specificity and palatability-relatedness of its taste responses—is a function of its embeddedness in the reciprocal circuit. Collectively, these results support our argument that the BLA/GC dyad behaves, probably because of the direct recurrent connectivity between the two regions, as a joint attractor network, processing tastes by collectively transitioning through quasi-stable states.

These results highlight general principles that, we argue, are probably at work in other sensory processing circuits. Specifically, it is reasonable to propose that, within any nominally sensory network, activity evolves in a distributed yet coordinated fashion that is not present "by default" but rather established in response to stimulus input, and that neurons involved in inter-region communication reliably play outsized roles in processing. The following sections discuss this proposal in further detail, specifically considering: 1) how stimulus-evoked metastable dynamics seen in the amygdala-cortical circuit are well-described as a distributed attractor network; 2) whether this conceptualization can be generalized to describe work from other sensory systems; 3) the fact that the "flow of influence" in tightly connected dynamical systems is likely to be asymmetric, with distinct dynamics of influence acting in concert with one another; and 4)

514 implications of the finding that neurons most deeply "embedded" in the task-relevant circuit show
515 the strongest task-related encoding.

516 Amygdala-cortical taste activity evolves as a joint attractor network

517 The metastable population dynamics that make up GC taste responses have already been
518 successfully modeled as an attractor network (28,40,63,64). Noise-driven attractor hopping (28,40)
519 has recapitulated many GC response characteristics—the exponential distribution of state
520 durations, activity in partially overlapping population pools, and distinct neural encoding in different
521 states—and has been shown to perform noisy decision-making better than the same network in an
522 "integration regime." Even a very simple instantiation of such a model, comprised of mutually
523 inhibitory neural populations, effectively captures the changing levels of LFP coherence observed
524 between population states (see Ref. #16, Fig. 10).

525 Our current results reveal that this attractor network is made up not just of GC, but of the dyad of GC
526 and BLA. As predicted by such a model, all but the initial transitions in taste-evoked activity happen,
527 on average, with lags that are distributed normally around zero, despite the fact that the regions are
528 connected by relatively long axons—a result that is difficult to explain using hierarchical/feedforward
529 models which, by construction, contain sources and sinks of influence (65–67). In a joint attractor
530 network, there is no "source" of transitions, which are triggered by coordination of the noise in the
531 system. And while there was some (inevitable) variability in the inference of the state transitions, this
532 did not preclude us from identifying the non-zero between-region lag that exists in the 1st transitions
533 expressed between GC and BLA (which is also the only transition uncorrelated between BLA and GC,
534 see 16). Thus, we argue that taste input causes the BLA-GC system to switch from resembling a
535 feedforward system to resembling a recurrent attractor network as processing unfolds.

Results from research on other sensory systems are consistent with these conclusions

Evidence supporting our proposal that nominally separate regions may "coalesce" into a single perceptual processing unit abounds in research on other sensory systems. Work from Gaillard and Dehaene (68,69), for instance, reveals properties of the processing of visual stimuli that are qualitatively similar to the state transitions we see in taste processing. According to the model that these authors use to explain their data, Global Workplace Theory (GWT), sensory information is first transmitted in a feedforward manner to specific brain regions; activation of these regions then engages a distributed network via reciprocal projections, which essentially binds the regions together.

In Gaillard and Dehaene's GWT analysis, as in our analyses, different states reflect different stages of perceptual processing and transitions to different stages are determined by different mechanisms. Of particular relevance, their 2nd state is driven by recurrent interactions, is internally driven (as opposed to being stimulus-bound), and reflects "conscious" stimulus processing. This mirrors work showing that the late taste-processing state "codes" the psychological variable of palatability—the variable that is used to make consumption decisions (26,64,70–73). It is also consistent with our demonstration that perturbation of the transition into this state most strongly impacts decision making with regard to consumption (Mukherjee 2019).

In work that even more concretely parallels our own (23), researchers recorded intracranial EEG from an ensemble of six cortical regions (early visual cortex, middle fusiform gyrus, pars triangularis, pars opercularis, ventral sensorimotor cortex, and auditory cortex). Using Hidden Markov Modeling on data collected as human subjects viewed and verbally identified pictures, the researchers demonstrated that these regions transition collectively through a sequence of 3 states: 1) a stimulus-

559 locked state lasting approximately 250ms, within which activity flows in a feedforward manner from
560 Early Visual Cortex to the other regions; 2) a variable-length pre-output state characterized by
561 distributed connectivity (i.e., with no single source or sink region; see also 74); and 3) an output state,
562 centered on the period 1000-1500ms post-stimulus delivery, during which behavioral responses are
563 released. This 3-state dynamic mirrors several features of responses (see **Fig. 1A**) observed during
564 awake tasting in rats: 1) the timings of state transitions, 2) the fact that these transitions occur across
565 a distributed set of brain regions behaving as a collective whole, and 3) the evolution of processing
566 from feedforward to strongly recurrent.

567 Supp et al. (75) provide converging evidence from still another system, in the form of analysis of EEG
568 responses to small wrist shocks in human subjects under different levels of anesthesia. These
569 responses were, in conscious subjects, characterized by an initial period of roughly 200ms in which
570 activity is primarily seen in the somatosensory cortex, followed by a second period of roughly 200ms
571 characterized by distributed activation of multiple cortical regions (a result suggesting long-range
572 interactions, although the coupling between regions was not explicitly tested). Anesthesia, which
573 diminishes the behavioral response to this painful stimulus, eliminates distributed activation of
574 regions in the second state without impacting activity in the first (feedforward) state, suggesting that
575 in this system as well the 2nd state is related to conscious processing.

576 The function(s) of BLA-GC directional influences

577 While BLA and GC progress through taste processing in lock-step, as is reasonable to expect given
578 the reciprocal connections between them, the manner with which each region influences the other
579 is asymmetric. It is actually not unusual (quite the opposite) for recurrently interacting systems to
580 contain such asymmetric influences. Examples of dynamical systems in which feedforward and
581 feedback interactions have different strengths include half-center oscillators (76), Lotka-Volterra

582 (prey-predator) models (77), and reservoir networks (78). Furthermore, researchers have reported
583 asymmetric interactions analogous to our own in data collected from visual system recordings
584 (19,21,50).

585 By Granger Causality (GrCa) analysis, the dynamics of the amygdala-cortical interaction accord well
586 with classic stimulus-valuation studies, including those performed by Damasio (Bechara 1999) and
587 Schoenbaum (Schoenbaum 1999), which have been interpreted as suggesting that amygdala, after
588 playing a primary role in determining the value of a stimulus, provides this information to cortex
589 which then uses the information to generate a behavioral decision. This interpretation is also
590 consistent with: 1) the fact that GC neurons primarily encode taste quality (discriminability,
591 (24,26,33) during the ~200-800msec middle epoch, at a time that BLA neurons are already
592 responding in a palatability-related manner (13,25); 2) the appearance of a peak in the GC→BLA
593 influence aligned with the average time of the transition into palatability-related firing in GC (just after
594 1000ms post-stimulus delivery); and 3) the role of this GC transition in driving behavioral responses
595 to the taste (26,34). Our GrCa analysis provides the first representation of this "signal" being emitted
596 by GC. In this context, however, it is worth noting that Forseth et al. (23) observed a similar transient
597 "signal" emanating from somatomotor regions approximately 250ms prior to the onset of response
598 articulation in the above-discussed visual-naming task.

599 Again, this analysis is consistent with our central suggestion that BLA and GC act not as separate
600 structures but rather as a single processing unit. Taste processing is not actually feedforward, but
601 rather emerges out of reciprocal interaction (see 9,69).

602 The role of projection neurons in sensory processing

603 The results of our Poisson General Linear Modeling (pGLM) make it clear that the GC neurons most
604 deeply involved in taste processing—quantified in terms of the magnitude of taste-specificity and

605 palatability-relatedness of their responses, basic response parameters that are summarized in our
606 "tastiness" metric—are those that both receive influence from and send influence to BLA.
607 Furthermore, the responses of GC neurons that are "simply" influenced by BLA (i.e., that don't also
608 influence BLA) are still more deeply taste- and palatability-specific than those that don't.

609 These results suggest that a breakdown of neuron types based on embeddedness in the reciprocal
610 circuit may be more meaningful for understanding function than more classically considered
611 subdivisions. Previous work has shown that while afferents from thalamus and BLA broadly overlap
612 in GC, the "hotspots" of these projections are visibly distinct (79). While our data do not directly test
613 this hypothesis, it is likely that some thalamocortical afferents, which are those carrying ascending
614 taste information, synapse on neurons that are not directly influenced by BLA; this consideration
615 carries with it the somewhat surprising realization that this ascending influence does not uniquely
616 determine the magnitude of taste responsiveness, but (in at least in a subset of neurons) taste
617 responsiveness is generated by a reciprocal interaction with amygdala (see (14) for a similar result
618 using cue-triggered responses). Furthermore, the pattern that we have observed is not well explained
619 by the unit's putative cell-type, suggesting that the "embedding" of the neuron in the circuit is more
620 significantly linked to function than morphology and molecular identity.

621 It is tempting to speculate that GC itself powers the processing attributed to BLA, perhaps by sending
622 taste quality information to BLA while BLA returns palatability information, with the two regions co-
623 evolving in this manner to converge to a decision (80). While GC neurons that influence BLA activity
624 without themselves being influenced by BLA activity (i.e., GC Output neurons) showed little or no
625 taste coding, the above conclusion can nonetheless be easily reconciled with previous work (8)
626 showing that a subset of GC→BLA projection neurons have more discriminatory taste-responses
627 compared to the average of non-projecting neurons, in response to aversive tastants vs palatable
628 tastants. These researchers showed that a subset of projection neurons more distinctly encode

629 valence than the average of non-projecting neurons. We predict that this subset of strongly
630 discriminatory GC→BLA projection neurons observed by Lavi et al. (8) were those deeply embedded
631 in the reciprocal circuit, that is, Input/Output neurons (although it is also possible that the fact that
632 Lavi et al. were examining responses in the context of CTA learning, which involves both GC and BLA,
633 may have changed functional connectivity).

634 This interpretation of BLA-GC "co-determination" is further supported by combining our GrCa results
635 with previous work (15) showing that pharmacological inhibition of taste thalamus suppressed 20-
636 60Hz LFP power in GC – exactly the band that dominates GC→BLA influence. Hence, and as noted
637 above, GC→BLA influence in this range may indicate simultaneous participation of GC in a parallel
638 circuit, likely the thalamocortical circuit, implicating the larger taste circuit in BLA-GC dynamics. In
639 future investigations we will directly test whether activity in GC→BLA axons, perhaps even activity
640 specifically confined to the γ-frequency range in which the GC→BLA influence is strongest, is
641 necessary for the evolution of amygdala-cortical taste processing (81).

642 Finally, there is evidence from studies examining other circuits (82–84) suggesting enhanced coding
643 in projection populations compared to non-projecting neurons. This may be rationalized from the
644 perspective that task-specific computations invoke different circuit configurations, therefore
645 different projections populations will be involved in specific tasks and neurons involved in the task-
646 relevant circuit will have the strongest encoding, as we observe in our results.

647 Conclusion

648 Our study reveals that cortico-amygdalar interactions subserve taste processing (and thereby taste
649 decision-making), showing that mechanisms previously theorized to underly state transitions in
650 cortical stimulus-evoked activity (attractor networks) are in fact part and parcel of the dynamics of
651 the GC-BLA dyad. By extension, we speculate that these dynamics are potentially a function of the

652 lager taste circuit including the brainstem (85). This taste network is initialized in a feedforward state
653 but coalesces into a reciprocally interacting network that evolves toward a point shown previously to
654 generate the behavioral output. Finally, our investigation of the makeup of GC Input and Output
655 neurons suggests that network interactions are stronger determinants of neural encoding than are
656 specific cell-types. All results presented herein align with previous studies from other sensory
657 systems as well as investigations of GC-BLA interactions during learning, allowing us to
658 conceptualize these previous results in a unified theoretical framework.

Methods

Experimental Design and Statistical Analyses

Subjects

Adult, female Long-Evans rats (n = 6; 300–350g at time of electrode implantation, Charles River Laboratories) served as subjects in our study (we have observed no sex differences in the basic cortical dynamics of taste responses between male and female rats, and therefore use female Long-Evans rats because they are, in our hands, calmer than males). The rats were housed in individual cages in a temperature- and humidity-controlled environment under a 12:12 hr light:dark cycle, given ad libitum access to food and water prior to the start of experimentation, and weighed daily following surgery to ensure that they never dropped below 80% of their pre-surgery weight. All experimental methods were in compliance with National Institutes of Health guidelines and were approved in advance by the Brandeis University Institutional Animal Care and Use Committee.

Electrode and intra-oral cannula construction

Custom microwire bundle drives, optimized for chronic (i.e., multi-day and multi-week) recording quality, were made with either 16 or 32 electrodes per recording site (design and construction details available at https://katzlab.squarespace.com/technology). Intra-oral cannulae—flexible tubing with a flanged tip and washer to ensure stability, connected to a plastic top complete with a locking mechanism—were built to allow the delivery of tastants directly onto the tongue (86).

677 ## Surgery

678 Rats were anaesthetized with an intraperitoneal injection of ketamine/xylazine cocktail (100mg/kg
679 and 5.2 mg/kg respectively) and mounted in a stereotaxic instrument (David Kopf Instruments;
680 Tujunga, CA) with blunt (atraumatic) ear bars. A midline incision exposed the skull and trephine holes
681 (~2 mm diameter) were drilled above BLA and GC. Microwire bundles were implanted 0.5mm above
682 GC (coordinates: AP +1.4 mm, ML -5.0 mm, DV −4.4mm from dura) and BLA (coordinates : AP -
683 3.0mm, ML -5.0mm, DV -6.8mm from dura). Once in place, electrode bundles were cemented to the
684 skull. Once electrode bundles were secured, an intra-oral cannula (IOC) was threaded through the
685 masseter muscle (inside the zygomatic arch) to the space between the lip and gums, and the top of
686 the cannula was cemented to the rest of the assembly with dental acrylic (Fontanini and Katz, 2006).
687 The rat's body temperature was monitored and maintained at ~37°C by a heating pad throughout the
688 duration of the surgery.

689 ## Acquisition of electrophysiological data

690 Electrophysiological signals from the micro-electrodes were sampled at 30 kHz using 32-channel
691 analog-to-digital converter chips (RHD2132) from Intan Technologies, digitized online at the head
692 stage and sampled jointly, along with signals from actuators marking tastant delivery, using an Intan
693 RHD USB interface board (Part #C3100), which routed records to the hard drive of a PC for saving.
694 The experimental chamber was ensconced in a Faraday cage that shielded recordings from external
695 electromagnetic influences.

696 ## Habituation and passive taste administration

697 Following their recovery from surgery, we habituated rats to the experimental chamber for 2 days, to
698 the IOC/electrode harness for the next 2 days, and to passive water deliveries for the following 2 days,

699 before beginning data collection. Starting with the second habituation day, we also placed rats on a
700 mild water restriction schedule—20mL of water (not including the ~4mL delivered during habituation
701 sessions themselves) per day. This water restriction schedule was maintained till the end of the
702 experiment. For the 2 final habituation sessions, we attached the rats to the taste delivery apparatus,
703 and infused 120 pulses of distilled water (~30μL per pulse; 20s inter-pulse interval) into the animal's
704 oral cavity through the IOC, and drove electrode bundles deeper (by 250 μm) into target structures.
705 By the end of this procedure, the tips of the electrodes lay within GC and BLA. We then recorded taste
706 responses during 3-4 days of taste delivery sessions, between each of which the microwire bundle
707 was driven down approximately 60 μm. During these sessions, Sucrose (0.3M), Sodium Chloride
708 (0.1M), Citric Acid (0.1M), and Quinine (1mM), dissolved in ultra-pure water (~30μL per pulse; 20s
709 inter-pulse interval, 30 trials/tastant) were delivered to passive rats (i.e., no behavior was required to
710 elicit delivery). These concentrations were chosen to represent a range of hedonic values, and
711 because they are known to evoke robust responses in both GC and BLA (25,33).

712 Histology

713 In preparation for histology, rats were deeply anesthetized with an overdose of the ketamine/xylazine
714 mixture. We perfused the rats through the heart with 0.9% saline followed by 10% formalin and
715 harvested the brain. The brain tissue was incubated in a fixing mixture of 30% sucrose and 10%
716 formalin for 7 days before being sectioned into 50μm coronal slices on a sliding microtome (Leica
717 SM2010R, Leica Microsystems). Sections containing the electrode implant sites around GC and BLA
718 were imaged at 2x.

Data and statistical analyses

The analysis of data and statistical tests were performed using custom written software in Python as described below.

Local Field Potential processing and analysis

Filtering / power and phase extractions

LFPs were extracted from broadband digitized signals using a 2nd order bandpass Butterworth filter (1-300Hz), to de-emphasize spiking and emphasize frequencies typically of interest in such data. In order to avoid contamination from noise/artifacts on noisy/broken channels, only channels containing isolable single neurons (see below) were used for analyses. Signal was down sampled to 1000Hz to reduce computational load for downstream analyses.

We note that this filtering process is sufficient for analysis up to the maximum frequency shown in the Results section (that is, 100Hz), and is unlikely to be the reason we don't observe effects above 60Hz. First, a maximum frequency of 300Hz is sufficient for a Nyquist frequency for accurately detecting signals up to 150Hz. Secondly, we use a Butterworth filter, which is "maximally flat" (see scipy.signal.butter, 87) within the pass band and is even permissive of frequencies higher than 300Hz. Hence, signals with frequencies 100Hz or lower are unlikely to be lost due to filtering.

Spectral Granger Causality

Spectral Granger Causality was assessed between pairs of electrodes in GC and BLA using the Spectral Connectivity package (47). We selected for this analysis the electrodes from which activity was most similar to the mean activity for the region (smallest mean-squared error relative to the mean phase across all channels for each region; this selection of channels was constant for all trials

in a single analyzed session, and the same set of channels was used for all frequencies), to ensure reliable representation of each.

To satisfy the normality assumption for use of Granger Causality, signals from both electrodes were first preprocessed according to previously established criteria to remove outliers and "detrend" the data (88). Briefly:

1. Any trials with data points exceeding 3 Median Absolute Deviations calculated using all the trials, were removed
2. Linear detrending was performed on a single-trial basis (scipy.signal.detrend)
3. The temporal (single-trial) mean was subtracted from the data, and all data divided by the temporal standard deviation
4. Trial-averaged mean was subtracted, and all data divided by the trial-averaged standard deviation

Following preprocessing, the Augmented Dickey-Fuller test was run on each channel to confirm stationarity (normality) of the signal. All preprocessed data passed the test and hence was included in further analyses.

Using the preprocessed data, spectral granger causality was calculated using multitaper methods implemented in the Spectral Connectivity package. The default set of tapers (Slepian) was used. Specific parameters included:

- "sampling_frequency" = 1000 (Hz),
- "time_halfbandwitch_product" = 1
- "time_window_duration" = 0.3 (sec)
- "time_window_step" = 0.05 (sec)

Significance of the granger causality for each frequency-time bin on a single-session basis was obtained using a shuffling procedure. Granger Causality was recalculated for 500 sets of data where trial labels were shuffled (mismatched) between BLA and GC to generate a null distribution of "non-specific" Granger Causality between the two regions. Deviation of the value in each frequency-time bin from its respective null distribution was taken to indicate a significant interaction in that bin. Multiple comparisons were addressed using the Bonferroni correction with a base alpha of 0.05 with each frequency-time bin treated as a comparison. We further supplemented this "bin-level" testing as below.

Cluster Permutation Testing

To perform statistical testing on the Granger Causality results while minimizing issues of multiple comparisons, we opted to use a cluster-based permutation test (89,90) to detect the largest statistically-significant deviation in the time-series for the 0-12Hz and 20-60Hz frequency bands. Briefly, the procedure involves:

1. Z-scoring the time-series on which testing needs to be done (in our case, this is the mean significance of Granger Causality for a frequency band)
2. Assessing the summed value of the largest cluster (continuous chunk) above a specific threshold for the absolute of the z-scored time-series (we used a threshold of Z = 2). This value is used as the test statistic.
3. This summed value of the largest cluster is then recalculated from shuffled data to obtain a null-distribution for the test statistic.
4. If the actual value of the statistic significantly deviates from the null-distribution, the null hypothesis is rejected (alpha=0.05).

Granger Causality Similarity Analysis

To analyze similarities in the dynamics of the directional Granger Causality timeseries, we performed Principal Component Analysis on the Granger Causality significance timeseries for 0-100Hz, reducing each multivariate timeseries down to 3 components to mitigate overfitting in the following regression analyses. All comparisons were then performed on these dimensionally reduced timeseries. We next performed 1) Linear Regression between the two timeseries, 2) Linear regression between circularly (temporally) shuffled versions of the two timeseries (as a negative control / context for poor prediction), 3) Linear Autoregression, and 4) non-Linear Autoregression (Multilayered perceptron regressor, (91). For both forms of autoregression, we used the previous 3 timepoints to predict the current one. To obtain an estimate of the uncertainty of prediction, we performed bootstrapping of the data with 500 reruns of model fitting and prediction.

Analysis of Spiking Activity

Single Unit Isolation

Spikes from electrophysiological recordings were sorted and analyzed off-line using an in-house Python-based pipeline (92). Putative single-neuron waveforms with >5:1 signal-to-noise ratio (median absolute deviation) were sorted using a semi-supervised algorithm: recorded voltage data were filtered between 300-3000Hz, grouped into potential clusters by a Gaussian Mixture Models (GMM) fit to multiple waveform features; clusters were then labeled and/or refined manually (to increase conservatism) by the experimenters.

Single Unit Evoked Response Characterization

Evaluating single-neuron response taste specificity. To statistically determine the degree to which a single neuron's response contained taste-specific information, firing rates were estimated by convolving spike-trains with a rectangular window (length: 200ms). A one-way ANOVA (between

807 tastes, across trials) was then run on each window to identify if the response of a single neuron to
808 one taste was different from its responses to any other tastes at that timepoint. The (taste) specificity
809 of a single neuron was defined as the average of the ANOVA effect sizes for 2000ms of post-stimulus
810 activity.

811 Evaluating single-neuron response palatability-relatedness. To statistically determine the degree to
812 which a single neuron's response reflected the hedonic value of the stimuli delivered, we estimated
813 firing rates as described above, and calculated the Pearson's correlation coefficient between the
814 evoked firing rates and the palatability ranks of the tastants at each timepoint. Palatability ranks —
815 sucrose (1) > NaCl (2) > citric acid (3) > quinine (4) — directly reflected consumption of (earlier-run
816 squads of) rats in a Brief Access Task (see 33). This ordering is canonical, and has been replicated in
817 many studies and with multiple measures of stimulus appreciation (86,93,94). The palatability of a
818 single neuron was defined as the average of the absolute correlation value (as the correlation can
819 also be strongly negative) for 2000ms of post-stimulus activity.

820 Calculating "Tastiness"

821 To combine taste specificity and palatability into a single metric, we first log-transformed specificity
822 to make the scales of specific and palatability more similar. This is because palatability as an
823 absolute value of a correlation is bounded between [0,1] whereas specificity as an effect size has the
824 range [0, ∞). Log-Specificity and Palatability were then Min-Max normalized following which the L2-
825 norm of the vector generated by the normalized metrics (normalized log-specificity, normalized
826 palatability) was calculated on a single-neuron basis and defined as "tastiness".

827 *Determination of putative pyramidal vs inter-neurons*

828 From the average of filtered spikes for each putative single-unit, we determined the time taken from
829 the trough to the next peak. As established previously, inter-neurons and pyramidal neurons can be

830 reliably separated using this “rise time” (11,58–60). The specific threshold varies depending on the
831 filtering frequencies used. We used a value of 0.45ms based on previous work using the same
832 bandpass filter frequencies as we have used here (11,60)

833 Changepoint Modeling of Population Activity

834 *Model Fitting*

835 Changepoint modelling of neural activity was performed as described previously (95) using the pytau
836 library (https://github.com/abuzarmahmood/pytau) written in Python. Briefly, spike-trains were
837 binned into 50ms bins. Changepoint models with independent Poisson emissions were fit to these
838 timeseries of binned spike-counts for BLA and GC populations separately using automatic
839 differentiation variational inference (ADVI) functionalities implemented in the pymc3 probabilistic
840 programming library (96). Once fit, the procedure returns: 1) the estimate of the posterior distribution
841 for single-trial population changepoint locations, and 2) the emission (firing) rates for each neuron
842 during every state. Since ADVI utilizes spherical Gaussians as the surrogate distribution, we use the
843 mode of the distribution for individual parameters as the “best estimate” of the parameter for
844 downstream analyses. Models with 4 states were fit to 2000ms of post-stimulus activity. Please refer
845 to (95) for more details on the process of model/state-number selection.

846 *Calculation of Transition Lags*

847 Lags between BLA and GC transitions were calculated on a single-trial basis by subtracting the “best
848 estimate” (see above) of the matched transition (that is, transition 1 in GC was compared to transition
849 1 in BLA for any given trial) between models fit to each region. This resulted in a distribution of lags
850 for each recording session (120 values, 1 for each trial in a session). The means of each session’s
851 distribution were used to generate a distribution of average lags for each transition across all the
852 recording sessions. Finally, a grand average of each transition’s distribution of average lags was

calculated. The significance of the deviation of this grand-average lag from zero was calculated by bootstrapping at the level of trials for each session with a total of 5000 permutations. The 95% confidence interval of each grand average was calculated using these bootstrapped distributions, and deviation of zero from this 95% interval was taken as a significant difference.

Generalized Linear Modelling

As has been shown previously, Granger Causality methods perform poorly on spike-train data due to the strong violation of the stationarity assumption used by the autoregressive processes on which Granger Causality is based (97,98). This issue is addressed by Generalized Linear Models (GLM; distinct from General Linear Models which also follow the stationarity/normality assumption) which can model Poisson-distributed data, and furthermore can model temporal dependencies explicitly over a large range of timescales (54,66,99,100).

Model Specification and Model Fitting

The GLM included 3 sets of filters for each neuron modelled:

- Spike History Filter: Captures how a neuron's past spiking activity influences its current firing rate. This can model refractoriness (reduced probability of firing immediately after a spike) and bursting behavior.
- Stimulus Filter: Models how external stimuli drive neural activity.
- Coupling Filter: Captures how the activity of other neurons influences the target neuron, modeling functional connectivity.

The duration of the spike history and coupling filters was set to 100ms, while the duration of the stimulus filter was set to 300ms, based on previous modelling work (54). To reduce number of fit parameters and mitigate over-fitting of the models, raised cosine-basis functions were used to

875 parameterize the filters (54,55,99): a basis of 10 functions was used for every filter, with peaks
876 distributed logarithmically to model fast and slow timescales with appropriate temporal resolutions.

877 The conditional intensity of the neural activity was hence defined as:

878 $\lambda(t) = \exp(\beta_0 + \beta_hist * h(t) + \beta_stim * s(t) + \beta_coup * c(t))$

879 - $\lambda(t)$ is the firing rate at time t
880 - β_0 is the baseline firing rate
881 - h(t) represents the neuron's own spike history
882 - s(t) represents the stimulus
883 - c(t) represents the coupling with other neurons
884 - β terms are the corresponding weights

885 The Python "statsmodels" library was used for model fitting (101).

886 Quality of fit was assessed in two ways. First, by comparing the log-likelihood of models fit to actual
887 data with models fit to data where the trial labels were shuffled for neurons in the ensemble being
888 fit, which would only allow the model to learn an "average" coupling filter between the neurons in the
889 model being fit. Second, we compared Spearman's Rho between predicted peri-stimulus time
890 histograms (PSTH) of a given neuron with PSTHs predicted for 1) the neuron the model was fit to
891 (actual data), 2) a different neuron (Unit Shuffled), and 3) temporally scrambled data for the same
892 neuron (Circular Shuffle).

893 Once models were fit, putative inter-neuron connections were determined using the coupling filters
894 between neurons. The fitting process returns p-values for each coefficient in the coupling filter
895 (which, in our case due to the parametrization of the filter using basis functions corresponded to the
896 scaling factor of each function in the basis). We asserted that a coupling filter indicated a statistically

significant interaction if a p-value in the filter was below alpha=0.05 following a Bonferroni correction (corrected p-value = 0.05 / 10 = 0.005).

Assessment of overlap between input and output populations

We assess whether the overlap observed between subpopulations labelled as “Input” and “Output” in GC and BLA was different from that expected by chance using Monte Carlo simulations. Essentially, keeping the number of Input, Output, and Total number of neurons in each region constant, we label neurons as Input or Output randomly and assess the number of neurons with both labels. We perform 10,000 simulations for each region to generate a null distribution for this overlap as expected by random assignment. Deviation of the observed value of overlap from the 2.5-97.5 percentile range of this distribution would indicate that the observed value is significantly different from that expected by chance with an alpha=0.05.

Data Availability

We have structured our electrophysiology datasets in a hierarchical data format (HDF5) and are hosting the files on a university-wide network share managed by Library and Technology Services (LTS) at Brandeis University. These HDF5 files contain our electrophysiology recordings, sorted spikes, single-neuron and population-level analyses (and associated plots and results). These files are prohibitively large to be hosted on a general-purpose fileshare platform - we request anyone interested in our datasets to contact the corresponding author, Donald Katz (dbkatz@brandeis.edu) who can put them in touch with LTS in order to create a guest account at Brandeis through which they can securely access our datasets (hosted on the katz-lab share at files.brandeis.edu).

References

1. Yarmolinsky DA, Zuker CS, Ryba NJP. Common Sense about Taste: From Mammals to Insects. Cell. 2009 Oct 16;139(2):234–44.

2. Carleton A, Accolla R, Simon SA. Coding in the mammalian gustatory system. Trends in Neurosciences. 2010 Jul 1;33(7):326–34.

3. Rolls ET. Taste and smell processing in the brain. In: Handbook of Clinical Neurology [Internet]. Elsevier; 2019 [cited 2025 Jan 19]. p. 97–118. Available from: https://linkinghub.elsevier.com/retrieve/pii/B9780444638557000071

4. Kietzmann TC, Spoerer CJ, Sörensen LKA, Cichy RM, Hauk O, Kriegeskorte N. Recurrence is required to capture the representational dynamics of the human visual system. Proceedings of the National Academy of Sciences. 2019 Oct 22;116(43):21854–63.

5. van Bergen RS, Kriegeskorte N. Going in circles is the way forward: the role of recurrence in visual inference. Current Opinion in Neurobiology. 2020 Dec 1;65:176–93.

6. Kriegeskorte N. Deep Neural Networks: A New Framework for Modeling Biological Vision and Brain Information Processing. Annual Review of Vision Science. 2015;1(1):417–46.

7. Piette CE, Baez-Santiago MA, Reid EE, Katz DB, Moran A. Inactivation of Basolateral Amygdala Specifically Eliminates Palatability-Related Information in Cortical Sensory Responses. J Neurosci. 2012 Jul 18;32(29):9981–91.

8. Lavi K, Jacobson GA, Rosenblum K, Lüthi A. Encoding of Conditioned Taste Aversion in Cortico-Amygdala Circuits. Cell Reports. 2018 Jul 10;24(2):278–83.

9. Kayyal H, Yiannakas A, Chandran SK, Khamaisy M, Sharma V, Rosenblum K. Activity of Insula to Basolateral Amygdala Projecting Neurons is Necessary and Sufficient for Taste Valence Representation. J Neurosci. 2019 Nov 20;39(47):9369–82.

10. Arieli E, Gerbi R, Shein-Idelson M, Moran A. Temporally-precise basolateral amygdala activation is required for the formation of taste memories in gustatory cortex. The Journal of Physiology. 2020;598(23):5505–22.

11. Lin JY, Mukherjee N, Bernstein MJ, Katz DB. Perturbation of amygdala-cortical projections reduces ensemble coherence of palatability coding in gustatory cortex. Schoenbaum G, Wassum KM, editors. eLife. 2021 May 21;10:e65766.

12. Yiannakas A, Kolatt Chandran S, Kayyal H, Gould N, Khamaisy M, Rosenblum K. Parvalbumin interneuron inhibition onto anterior insula neurons projecting to the basolateral amygdala drives aversive taste memory retrieval. Current Biology. 2021 Jul 12;31(13):2770-2784.e6.

13. Grossman SE, Fontanini A, Wieskopf JS, Katz DB. Learning-Related Plasticity of Temporal Coding in Simultaneously Recorded Amygdala–Cortical Ensembles. J Neurosci. 2008 Mar 12;28(11):2864–73.

14. Samuelsen CL, Gardner MPH, Fontanini A. Effects of Cue-Triggered Expectation on Cortical Processing of Taste. Neuron. 2012 Apr 26;74(2):410–22.

15. Samuelsen CL, Gardner MPH, Fontanini A. Thalamic Contribution to Cortical Processing of Taste and Expectation. J Neurosci. 2013 Jan 30;33(5):1815–27.

16. Mahmood A, Steindler J, Germaine H, Miller P, Katz DB. Coupled Dynamics of Stimulus-Evoked Gustatory Cortical and Basolateral Amygdalar Activity. J Neurosci. 2023 Jan 18;43(3):386–404.

17. Bressler SL, Coppola R, Nakamura R. Episodic multiregional cortical coherence at multiple frequencies during visual task performance. Nature. 1993 Nov;366(6451):153.

18. van Kerkoerle T, Self MW, Dagnino B, Gariel-Mathis MA, Poort J, van der Togt C, et al. Alpha and gamma oscillations characterize feedback and feedforward processing in monkey visual cortex. Proc Natl Acad Sci U S A. 2014 Oct 7;111(40):14332–41.

19. Bastos AM, Vezoli J, Bosman CA, Schoffelen JM, Oostenveld R, Dowdall JR, et al. Visual Areas Exert Feedforward and Feedback Influences through Distinct Frequency Channels. Neuron. 2015 Jan 21;85(2):390–401.

20. Arce-McShane FI, Ross CF, Takahashi K, Sessle BJ, Hatsopoulos NG. Primary motor and sensory cortical areas communicate via spatiotemporally coordinated networks at multiple frequencies. Proceedings of the National Academy of Sciences. 2016 May 3;113(18):5083–8.

21. Mejias JF, Murray JD, Kennedy H, Wang XJ. Feedforward and feedback frequency-dependent interactions in a large-scale laminar network of the primate cortex. Science Advances. 2016 Nov 1;2(11):e1601335.

22. Michaels JA, Dann B, Scherberger H. Neural Population Dynamics during Reaching Are Better Explained by a Dynamical System than Representational Tuning. PLOS Computational Biology. 2016 Nov 4;12(11):e1005175.

23. Saravani AG, Forseth KJ, Tandon N, Pitkow X. Dynamic Brain Interactions during Picture Naming. eNeuro [Internet]. 2019 Jul 1 [cited 2020 Feb 16];6(4). Available from: https://www.eneuro.org/content/6/4/ENEURO.0472-18.2019

24. Katz DB, Simon SA, Nicolelis MAL. Dynamic and Multimodal Responses of Gustatory Cortical Neurons in Awake Rats. J Neurosci. 2001 Jun 15;21(12):4478–89.

25. Fontanini A, Grossman SE, Figueroa JA, Katz DB. Distinct Subtypes of Basolateral Amygdala Taste Neurons Reflect Palatability and Reward. J Neurosci. 2009 Feb 25;29(8):2486–95.

26. Sadacca BF, Mukherjee N, Vladusich T, Li JX, Katz DB, Miller P. The Behavioral Relevance of Cortical Neural Ensemble Responses Emerges Suddenly. J Neurosci. 2016 Jan 20;36(3):655–69.

27. Hopfield JJ. Neural networks and physical systems with emergent collective computational abilities. PNAS. 1982 Apr 1;79(8):2554–8.

28. Miller P, Katz DB. Stochastic Transitions between Neural States in Taste Processing and Decision-Making. J Neurosci. 2010 Feb 17;30(7):2559–70.

29. McDonald AJ. Cortical pathways to the mammalian amygdala. Progress in Neurobiology. 1998 Jun 27;55(3):257–332.

30. Shi CJ, Cassell MD. Cortical, thalamic, and amygdaloid connections of the anterior and posterior insular cortices. The Journal of Comparative Neurology. 1998 Oct 5;399(4):440–68.

31. Stone ME, Maffei A, Fontanini A. Amygdala Stimulation Evokes Time-Varying Synaptic Responses in the Gustatory Cortex of Anesthetized Rats. Front Integr Neurosci [Internet]. 2011 [cited 2019 May 8];5. Available from: https://www.frontiersin.org/articles/10.3389/fnint.2011.00003/full

32. Haley MS, Fontanini A, Maffei A. Laminar- and Target-Specific Amygdalar Inputs in Rat Primary Gustatory Cortex. J Neurosci. 2016 Mar 2;36(9):2623–37.

33. Sadacca BF, Rothwax JT, Katz DB. Sodium Concentration Coding Gives Way to Evaluative Coding in Cortex and Amygdala. J Neurosci. 2012 Jul 18;32(29):9999–10011.

34. Mukherjee N, Wachutka J, Katz DB. Impact of precisely-timed inhibition of gustatory cortex on taste behavior depends on single-trial ensemble dynamics. Colgin LL, Maffei A, Maffei A, Ghazanfar AA, Verhagen J, Mazzucato L, editors. eLife. 2019 Jun 24;8:e45968.

35. Fontanini A, Katz DB. 7 to 12 Hz Activity in Rat Gustatory Cortex Reflects Disengagement From a Fluid Self-Administration Task. Journal of Neurophysiology. 2005 May 1;93(5):2832–40.

36. Tort ABL, Fontanini A, Kramer MA, Jones-Lush LM, Kopell NJ, Katz DB. Cortical Networks Produce Three Distinct 7–12 Hz Rhythms during Single Sensory Responses in the Awake Rat. J Neurosci. 2010 Mar 24;30(12):4315–24.

37. Pavão R, Piette CE, Lopes-dos-Santos V, Katz DB, Tort ABL. Local Field Potentials in the Gustatory Cortex Carry Taste Information. J Neurosci. 2014 Jun 25;34(26):8778–87.

38. Moran A, Katz DB. Sensory Cortical Population Dynamics Uniquely Track Behavior across Learning and Extinction. J Neurosci. 2014 Jan 22;34(4):1248–57.

39. Bell T. Attractor transitions: A basis for sequential processing in neural networks? Neural Networks. 1988;1:163.

40. Miller P, Katz DB. Accuracy and response-time distributions for decision-making: linear perfect integrators versus nonlinear attractor-based neural circuits. J Comput Neurosci. 2013 Dec 1;35(3):261–94.

41. Brennan C, Proekt A. Attractor dynamics with activity-dependent plasticity capture human working memory across time scales. Commun Psychol. 2023 Oct 25;1(1):1–15.

42. Jones LM, Fontanini A, Sadacca BF, Miller P, Katz DB. Natural stimuli evoke dynamic sequences of states in sensory cortical ensembles. PNAS. 2007 Nov 20;104(47):18772–7.

43. Ding M, Chen Y, Bressler SL. Granger Causality: Basic Theory and Application to Neuroscience [Internet]. arXiv; 2006 [cited 2023 Apr 26]. Available from: http://arxiv.org/abs/q-bio/0608035

44. Seth AK, Barrett AB, Barnett L. Granger causality analysis in neuroscience and neuroimaging. J Neurosci. 2015 Feb 25;35(8):3293–7.

45. Geweke J. Measurement of Linear Dependence and Feedback Between Multiple Time Series. Journal of the American Statistical Association. 1982;77(378):304–13.

46. Chicharro D. On the spectral formulation of Granger causality. Biol Cybern. 2011 Dec;105(5–6):331–47.

47. Denovellis EL, Myroshnychenko M, Sarmashghi M, Stephen EP. Spectral Connectivity: a python package for computing multitaper spectral estimates and frequency-domain brain connectivity measures on the CPU and GPU. Journal of Open Source Software. 2022 Dec 13;7(80):4840.

48. Buzsáki G, Draguhn A. Neuronal Oscillations in Cortical Networks. Science. 2004 Jun 25;304(5679):1926–9.

49. Baccalá LA, Sameshima K. Partial directed coherence: a new concept in neural structure determination. Biol Cybern. 2001 May 1;84(6):463–74.

50. Arce-McShane FI, Ross CF, Takahashi K, Sessle BJ, Hatsopoulos NG. Primary motor and sensory cortical areas communicate via spatiotemporally coordinated networks at multiple frequencies. PNAS. 2016 Apr 15;201600788.

51. Bechara A, Damasio H, Damasio AR, Lee GP. Different Contributions of the Human Amygdala and Ventromedial Prefrontal Cortex to Decision-Making. J Neurosci. 1999 Jul 1;19(13):5473–81.

52. Schoenbaum G, Chiba AA, Gallagher M. Neural Encoding in Orbitofrontal Cortex and Basolateral Amygdala during Olfactory Discrimination Learning. J Neurosci. 1999 Mar 1;19(5):1876–84.

53. Michalareas G, Vezoli J, van Pelt S, Schoffelen JM, Kennedy H, Fries P. Alpha-Beta and Gamma Rhythms Subserve Feedback and Feedforward Influences among Human Visual Cortical Areas. Neuron. 2016 Jan 20;89(2):384–97.

54. Pillow JW, Shlens J, Paninski L, Sher A, Litke AM, Chichilnisky EJ, et al. Spatio-temporal correlations and visual signalling in a complete neuronal population. Nature. 2008 Aug;454(7207):995–9.

55. Stevenson IH, Rebesco JM, Miller LE, Körding KP. Inferring functional connections between neurons. Curr Opin Neurobiol. 2008 Dec;18(6):582–8.

56. Magrans de Abril I, Yoshimoto J, Doya K. Connectivity inference from neural recording data: Challenges, mathematical bases and research directions. Neural Networks. 2018 Jun 1;102:120–37.

57. Kobayashi R, Kurita S, Kurth A, Kitano K, Mizuseki K, Diesmann M, et al. Reconstructing neuronal circuitry from parallel spike trains. Nat Commun. 2019 Oct 2;10(1):4468.

58. Sirota A, Montgomery S, Fujisawa S, Isomura Y, Zugaro M, Buzsáki G. Entrainment of Neocortical Neurons and Gamma Oscillations by the Hippocampal Theta Rhythm. Neuron. 2008 Nov 26;60(4):683–97.

1060 59. Quirk MC, Sosulski DL, Feierstein CE, Uchida N, Mainen ZF. A defined network of fast-spiking
1061 interneurons in orbitofrontal cortex: responses to behavioral contingencies and ketamine
1062 administration. Front Syst Neurosci [Internet]. 2009 Nov 3 [cited 2025 May 8];3. Available from:
1063 https://www.frontiersin.orghttps://www.frontiersin.org/journals/systems-
1064 neuroscience/articles/10.3389/neuro.06.013.2009/full

1065 60. Herzog LE, Pascual LM, Scott SJ, Mathieson ER, Katz DB, Jadhav SP. Interaction of Taste and
1066 Place Coding in the Hippocampus. J Neurosci. 2019 Apr 17;39(16):3057–69.

1067 61. Li JX, Yoshida T, Monk KJ, Katz DB. Lateral Hypothalamus Contains Two Types of Palatability-
1068 Related Taste Responses with Distinct Dynamics. J Neurosci. 2013 May 29;33(22):9462–73.

1069 62. Kosar E, Grill HJ, Norgren R. Gustatory cortex in the rat. II. Thalamocortical projections. Brain
1070 Research. 1986 Aug 6;379(2):342–52.

1071 63. Mazzucato L, Fontanini A, Camera GL. Dynamics of Multistable States during Ongoing and
1072 Evoked Cortical Activity. J Neurosci. 2015 May 27;35(21):8214–31.

1073 64. Lang L, Camera GL, Fontanini A. Temporal progression along discrete coding states during
1074 decision-making in the mouse gustatory cortex. PLOS Computational Biology. 2023 Feb
1075 7;19(2):e1010865.

1076 65. Parras GG, Nieto-Diego J, Carbajal GV, Valdés-Baizabal C, Escera C, Malmierca MS. Neurons
1077 along the auditory pathway exhibit a hierarchical organization of prediction error. Nat Commun.
1078 2017 Dec 15;8(1):2148.

66. Glaser JI, Perich MG, Ramkumar P, Miller LE, Kording KP. Population coding of conditional probability distributions in dorsal premotor cortex. Nature Communications. 2018 May 3;9(1):1–14.

67. Heidari-Gorji H, Ebrahimpour R, Zabbah S. A temporal hierarchical feedforward model explains both the time and the accuracy of object recognition. Sci Rep. 2021 Mar 11;11(1):5640.

68. Dehaene S, Sergent C, Changeux JP. A neuronal network model linking subjective reports and objective physiological data during conscious perception. Proceedings of the National Academy of Sciences. 2003 Jul 8;100(14):8520–5.

69. Gaillard R, Dehaene S, Adam C, Clémenceau S, Hasboun D, Baulac M, et al. Converging Intracranial Markers of Conscious Access. PLOS Biology. 2009 Mar 17;7(3):e1000061.

70. Rogers PJ. Why a palatability construct is needed. Appetite. 1990 Jun;14(3):167–70; discussion 180.

71. Araujo JA, Studzinski CM, Larson BT, Milgram NW. Comparison of the cognitive palatability assessment protocol and the two-pan test for use in assessing palatability of two similar foods in dogs. 2004 Nov 1 [cited 2025 May 6]; Available from: https://avmajournals.avma.org/view/journals/ajvr/65/11/ajvr.65.11.1490.xml

72. Breslin PAS. The Sense of Taste Encompasses Two Roles: Conscious Taste Perception and Subconscious Metabolic Responses. In: Think Tank [Internet]. Yale University Press; 2018 [cited 2025 May 6]. p. 110–8. Available from: https://www.degruyterbrill.com/document/doi/10.12987/9780300235470-017/html?srsltid=AfmBOopo1-t48Heuq2k_xlyWiTnwcA6QP4aYMaFChOt_KAeaiSt3OwPX

73. Vincis R, Chen K, Czarnecki L, Chen J, Fontanini A. Dynamic Representation of Taste-Related Decisions in the Gustatory Insular Cortex of Mice. Current Biology. 2020 May 18;30(10):1834-1844.e5.

74. Forseth KJ, Pitkow X, Fischer-Baum S, Tandon N. What The Brain Does As We Speak [Internet]. bioRxiv; 2021 [cited 2025 May 6]. p. 2021.02.05.429841. Available from: https://www.biorxiv.org/content/10.1101/2021.02.05.429841v1

75. Supp GG, Siegel M, Hipp JF, Engel AK. Cortical Hypersynchrony Predicts Breakdown of Sensory Processing during Loss of Consciousness. Current Biology. 2011 Dec 6;21(23):1988–93.

76. Skinner FK, Gramoll S, Calabrese RL, Kopell N, Marder E. Frequency Control in Biological Half-Center Oscillators. In: Eeckman FH, editor. Computation in Neurons and Neural Systems [Internet]. Boston, MA: Springer US; 1994 [cited 2025 May 6]. p. 223–8. Available from: https://doi.org/10.1007/978-1-4615-2714-5_36

77. Diz-Pita É, Otero-Espinar MV. Predator–Prey Models: A Review of Some Recent Advances. Mathematics. 2021 Jan;9(15):1783.

78. Vrugt M te. An introduction to reservoir computing [Internet]. arXiv; 2024 [cited 2025 May 6]. Available from: http://arxiv.org/abs/2412.13212

79. Stone ME, Fontanini A, Maffei A. Synaptic Integration of Thalamic and Limbic Inputs in Rodent Gustatory Cortex. eNeuro [Internet]. 2020 Jan 1 [cited 2025 May 8];7(1). Available from: https://www.eneuro.org/content/7/1/ENEURO.0199-19.2019

80. Ahissar E, Assa E. Perception as a closed-loop convergence process. Kleinfeld D, editor. eLife. 2016 May 9;5:e12830.

81. Jones SR, Kerr CE, Wan Q, Pritchett DL, Hämäläinen M, Moore CI. Cued Spatial Attention Drives Functionally Relevant Modulation of the Mu Rhythm in Primary Somatosensory Cortex. J Neurosci. 2010 Oct 13;30(41):13760–5.

82. Beyeler A, Chang CJ, Silvestre M, Lévêque C, Namburi P, Wildes CP, et al. Organization of Valence-Encoding and Projection-Defined Neurons in the Basolateral Amygdala. Cell Reports. 2018 Jan 23;22(4):905–18.

83. Lui JH, Nguyen ND, Grutzner SM, Darmanis S, Peixoto D, Wagner MJ, et al. Differential encoding in prefrontal cortex projection neuron classes across cognitive tasks. Cell. 2021 Jan 21;184(2):489-506.e26.

84. Gongwer MW, Klune CB, Couto J, Jin B, Enos AS, Chen R, et al. Brain-Wide Projections and Differential Encoding of Prefrontal Neuronal Classes Underlying Learned and Innate Threat Avoidance. J Neurosci. 2023 Aug 9;43(32):5810–30.

85. Baez-Santiago MA, Reid EE, Moran A, Maier JX, Marrero-Garcia Y, Katz DB. Dynamic taste responses of parabrachial pontine neurons in awake rats. Journal of Neurophysiology. 2016 Jan 20;115(3):1314–23.

86. Fontanini A, Katz DB. State-Dependent Modulation of Time-Varying Gustatory Responses. Journal of Neurophysiology. 2006 Dec 1;96(6):3183–93.

87. Virtanen P, Gommers R, Oliphant TE, Haberland M, Reddy T, Cournapeau D, et al. SciPy 1.0: fundamental algorithms for scientific computing in Python. Nat Methods. 2020 Mar;17(3):261–72.

88. Ding M, Bressler SL, Yang W, Liang H. Short-window spectral analysis of cortical event-related potentials by adaptive multivariate autoregressive modeling: data preprocessing, model validation, and variability assessment. Biol Cybern. 2000 Jun 1;83(1):35–45.

89. Maris E, Oostenveld R. Nonparametric statistical testing of EEG- and MEG-data. Journal of Neuroscience Methods. 2007 Aug 15;164(1):177–90.

90. Candia-Rivera D, Valenza G. Cluster permutation analysis for EEG series based on non-parametric Wilcoxon–Mann–Whitney statistical tests. SoftwareX. 2022 Jul 1;19:101170.

91. Pedregosa F, Varoquaux G, Gramfort A, Michel V, Thirion B, Grisel O, et al. Scikit-learn: Machine Learning in Python. J Mach Learn Res. 2011 Nov 1;12(null):2825–30.

92. Mahmood A, Mukherjee N, Stone B, Raymond M, Germaine H, Lin JY, et al. katzlabbrandeis/blech_clust: v1.1.0 [Internet]. Zenodo; 2025 [cited 2025 May 15]. Available from: https://zenodo.org/records/15175273

93. Clarke SNDA, Ossenkopp KP. Taste reactivity responses in rats: influence of sex and the estrous cycle. American Journal of Physiology-Regulatory, Integrative and Comparative Physiology. 1998 Mar;274(3):R718–24.

94. Travers JB, Norgren R. Electromyographic analysis of the ingestion and rejection of sapid stimuli in the rat. Behavioral Neuroscience. 1986;100:544–55.

95. Mahmood A, Steindler J, Germaine H, Miller P, Katz DB. Coupled Dynamics of Stimulus-Evoked Gustatory Cortical and Basolateral Amygdalar Activity. J Neurosci. 2023 Jan 18;43(3):386–404.

96. Salvatier J, Wiecki TV, Fonnesbeck C. Probabilistic programming in Python using PyMC3. PeerJ Comput Sci. 2016 Apr 6;2:e55.

97. Kispersky T, Gutierrez GJ, Marder E. Functional connectivity in a rhythmic inhibitory circuit using Granger causality. Neural Syst Circuits. 2011 May 25;1:9.

98. Gerhard F, Kispersky T, Gutierrez GJ, Marder E, Kramer M, Eden U. Successful Reconstruction of a Physiological Circuit with Known Connectivity from Spiking Activity Alone. PLOS Computational Biology. 2013 Jul 11;9(7):e1003138.

99. Stevenson IH, Rebesco JM, Hatsopoulos NG, Haga Z, Miller LE, Kording KP. Bayesian Inference of Functional Connectivity and Network Structure From Spikes. IEEE Transactions on Neural Systems and Rehabilitation Engineering. 2009 Jun;17(3):203–13.

100. Keeley SL, Zoltowski DM, Aoi MC, Pillow JW. Modeling statistical dependencies in multi-region spike train data. Current Opinion in Neurobiology. 2020 Dec 1;65:194–202.

101. Seabold S, Perktold J. Statsmodels: Econometric and Statistical Modeling with Python. In Austin, Texas; 2010 [cited 2025 May 16]. p. 92–6. Available from: https://doi.curvenote.com/10.25080/Majora-92bf1922-011